IEC TS 62791

Edition 2.0 2022-07

TECHNICAL SPECIFICATION

colour inside

Ultrasonics – Pulse-echo scanners – Low-echo sphere phantoms and method for performance testing of grey-scale medical ultrasound scanners applicable to a broad range of transducer types

IEC TS 62791:2022-07(en)

IEC Secretariat
3, rue de Varembé
CH-1211 Geneva 20
Switzerland

Tel.: +41 22 919 02 11
info@iec.ch
www.iec.ch

About the IEC
The International Electrotechnical Commission (IEC) is the leading global organization that prepares and publishes International Standards for all electrical, electronic and related technologies.

About IEC publications
The technical content of IEC publications is kept under constant review by the IEC. Please make sure that you have the latest edition, a corrigendum or an amendment might have been published.

IEC publications search - webstore.iec.ch/advsearchform
The advanced search enables to find IEC publications by a variety of criteria (reference number, text, technical committee, …). It also gives information on projects, replaced and withdrawn publications.

IEC Just Published - webstore.iec.ch/justpublished
Stay up to date on all new IEC publications. Just Published details all new publications released. Available online and once a month by email.

IEC Customer Service Centre - webstore.iec.ch/csc
If you wish to give us your feedback on this publication or need further assistance, please contact the Customer Service Centre: sales@iec.ch.

IEC Products & Services Portal - products.iec.ch
Discover our powerful search engine and read freely all the publications previews. With a subscription you will always have access to up to date content tailored to your needs.

Electropedia - www.electropedia.org
The world's leading online dictionary on electrotechnology, containing more than 22 300 terminological entries in English and French, with equivalent terms in 19 additional languages. Also known as the International Electrotechnical Vocabulary (IEV) online.

IEC TS 62791

Edition 2.0 2022-07

TECHNICAL SPECIFICATION

colour inside

Ultrasonics – Pulse-echo scanners – Low-echo sphere phantoms and method for performance testing of grey-scale medical ultrasound scanners applicable to a broad range of transducer types

INTERNATIONAL ELECTROTECHNICAL COMMISSION

ICS 11.040.50; 17.140.50

ISBN 978-2-8322-3922-3

CONTENTS

INTERNATIONAL ELECTROTECHNICAL COMMISSION

_____

ULTRASONICS – PULSE-ECHO SCANNERS – LOW-ECHO SPHERE PHANTOMS AND METHOD FOR PERFORMANCE TESTING OF GREY-SCALE MEDICAL ULTRASOUND SCANNERS APPLICABLE TO A BROAD RANGE OF TRANSDUCER TYPES

FOREWORD

1) The International Electrotechnical Commission (IEC) is a worldwide organization for standardization comprising all national electrotechnical committees (IEC National Committees). The object of IEC is to promote international co-operation on all questions concerning standardization in the electrical and electronic fields. To this end and in addition to other activities, IEC publishes International Standards, Technical Specifications, Technical Reports, Publicly Available Specifications (PAS) and Guides (hereafter referred to as "IEC Publication(s)"). Their preparation is entrusted to technical committees; any IEC National Committee interested in the subject dealt with may participate in this preparatory work. International, governmental and non-governmental organizations liaising with the IEC also participate in this preparation. IEC collaborates closely with the International Organization for Standardization (ISO) in accordance with conditions determined by agreement between the two organizations.
2) The formal decisions or agreements of IEC on technical matters express, as nearly as possible, an international consensus of opinion on the relevant subjects since each technical committee has representation from all interested IEC National Committees.
3) IEC Publications have the form of recommendations for international use and are accepted by IEC National Committees in that sense. While all reasonable efforts are made to ensure that the technical content of IEC Publications is accurate, IEC cannot be held responsible for the way in which they are used or for any misinterpretation by any end user.
4) In order to promote international uniformity, IEC National Committees undertake to apply IEC Publications transparently to the maximum extent possible in their national and regional publications. Any divergence between any IEC Publication and the corresponding national or regional publication shall be clearly indicated in the latter.
5) IEC itself does not provide any attestation of conformity. Independent certification bodies provide conformity assessment services and, in some areas, access to IEC marks of conformity. IEC is not responsible for any services carried out by independent certification bodies.
6) All users should ensure that they have the latest edition of this publication.
7) No liability shall attach to IEC or its directors, employees, servants or agents including individual experts and members of its technical committees and IEC National Committees for any personal injury, property damage or other damage of any nature whatsoever, whether direct or indirect, or for costs (including legal fees) and expenses arising out of the publication, use of, or reliance upon, this IEC Publication or any other IEC Publications.
8) Attention is drawn to the Normative references cited in this publication. Use of the referenced publications is indispensable for the correct application of this publication.
9) Attention is drawn to the possibility that some of the elements of this IEC Publication may be the subject of patent rights. IEC shall not be held responsible for identifying any or all such patent rights.

IEC TS 62791 has been prepared by IEC technical committee 87: Ultrasonics. It is a Technical Specification.

This second edition cancels and replaces the first edition published in 2015. This edition constitutes a technical revision.

This edition includes the following significant technical changes with respect to the previous edition.

a) It introduces necessary corrections to the analysis methods; these have been published in the literature.
b) It increases the range of contrast levels of **low-echo spheres** in phantoms that meet this Technical Specification. Previous specification was -20 dB, but two additional levels, -6 dB and either -30 dB or, if possible, -40 dB, are now specified.
c) It includes a wider range of uses of the methodology, including testing the effectiveness of scanner pre-sets for specific clinical tasks and detecting flaws in transducers and in beamforming.

d) It decreases the manufacturing cost by decreasing phantoms' dimensions and numbers of low-echo, backscattering spheres embedded in each phantom.

The text of this Technical Specification is based on the following documents:

Draft	Report on voting
87/776/DTS	87/790A/RVDTS

Full information on the voting for its approval can be found in the report on voting indicated in the above table.

The language used for the development of this Technical Specification is English.

This document was drafted in accordance with ISO/IEC Directives, Part 2, and developed in accordance with ISO/IEC Directives, Part 1 and ISO/IEC Directives, IEC Supplement, available at www.iec.ch/members_experts/refdocs. The main document types developed by IEC are described in greater detail at www.iec.ch/standardsdev/publications.

Terms in **bold** in the text are defined in Clause 3.

The committee has decided that the contents of this document will remain unchanged until the stability date indicated on the IEC website under webstore.iec.ch in the data related to the specific document. At this date, the document will be

- reconfirmed,
- withdrawn,
- replaced by a revised edition, or
- amended.

IMPORTANT – The "colour inside" logo on the cover page of this document indicates that it contains colours which are considered to be useful for the correct understanding of its contents. Users should therefore print this document using a colour printer.

INTRODUCTION

Ultrasonic pulse-echo scanners are widely used in medical practice to produce images of soft-tissue organs throughout the human body. Most ultrasonic pulse-echo scanners produce real-time images of tissue in a scan plane by sweeping a narrow, pulsed beam of ultrasound through the tissue section of interest and detecting the echoes generated by reflection at tissue boundaries and by scattering within tissues. Many newer scanners transmit broad, overlapping ultrasound beams, and apply software beam-forming to synthesize narrow, pulse-echo beam patterns.

Generally, the sweep that generates an image frame is repeated at least 20 times per second, giving rise to the real-time aspect of the displayed image. The axes of the pulsed beams generally lie in a plane that defines the scan plane.

Various transducer types are employed to operate in a transmit–receive mode to generate and detect the ultrasonic signals. Linear arrays, in which the beam axes are all parallel to one another, resulting in a rectangular image, consist of a line of hundreds of parallel transducer elements with a subset of adjacent elements producing one pulse at a time. Convex arrays are similar to linear arrays but the element arrangements define part of the surface of a short, right, circular cylinder with the array elements parallel to the axis of the cylinder. The radius of curvature of the cylinder (and therefore the array) can have values between 0,5 cm and 7 cm. The convex array generates a sector image, since the beam axes fan out over the scan plane. Some linear- and convex-array models, such as "1,25-D" arrays, incorporate multiple rows of elements to provide additional control of the elevational beam width.

A phased array has a linear arrangement of elements, where all elements act together to form a pulse and the direction and focus of an emitted pulse is determined by the timing of excitations of the elements. The phased array generates a sector image. Another type of sector scanner is the mechanical sector scanner in which a single-element transducer or an annular-array transducer is rotated about a fixed axis during pulse emissions. The foregoing transducer types commonly operate within the frequency range 1 MHz to 23 MHz, to which this document applies. Medical ultrasound systems exist whose transducers operate at frequencies as high as 33 MHz. Although the procedures specified in this document might be appropriate for these systems, phantoms outlined in this document have not yet been described for use in the 23 MHz to 33 MHz frequency range.

A two-dimensional array (2-D array) is restricted to an array of transducer elements distributed over a rectangular area or a spherical cap. Such an array receives echoes from a 3-D volume and can produce images corresponding to any planar surface in that volume. A 3-D mechanically driven, convex array (3-D MD convex array) means a convex array that acquires images as it is rotated mechanically about an axis lying in its **image plane** or an extension of that plane. A 3-D mechanically driven, linear array (3-D MD linear array) is similar to a 3-D MD convex array, where the array radius of curvature is infinite and the array is either rotated about an axis or is translated perpendicularly to the scan plane of the linear array. For an overview of current 3-D and 4-D systems, see 1.5 and 10.2.2 of [1][1].

One means for testing the imaging performance of an ultrasound pulse-echo scanner is to quantify the degree to which a small (low-echo) sphere is distinguished from the surrounding soft tissue, i.e. the degree to which a small, **low-echo sphere** is detectable in the surrounding soft tissue. It is reasonable to assume that the smaller the **low-echo sphere** that can be detected at some position, the better the resolution of the scanner, i.e. the better it will display and delineate the boundary of an abnormal object, such as a tumour, and the more accurately it will display local acoustic properties.

[1] Numbers in square brackets refer to the Bibliography.

There are three components of resolution defined in pulse-echo ultrasound:

– axial resolution (parallel to the local, pulse-propagation direction);
– lateral resolution (perpendicular to the local, pulse-propagation direction and parallel to the scan plane); and
– elevational resolution (perpendicular to the local, pulse-propagation direction and also to the scan plane).

Axial resolution usually – but not always – is better than lateral and elevational resolutions. Thus, all three components affect an object's **detectability**. A sphere has no preferred orientation and is therefore the best shape for assessing **detectability** of a low-echo object for two reasons. First, all three components of resolution are weighted equally, no matter what the beam's incident direction is. Second, the incident beam's propagation direction will vary considerably in the case of convex and phased arrays depending on where the object exists in the imaged volume.

Imaging performance can be reduced by:

- beam distortions associated with dead or weak elements in array transducers;
- side lobes and grating lobes that are present with some array transducers;
- unexpected beam changes accompanying variations in the transmit foci applied to multi-row ("1,25-D") arrays; and
- electronic noise.

All can contribute to artifactual echoes on clinical images and on images of phantoms containing **low-echo spheres** or to erroneous echo-signal amplitudes.

It is important that the phantom allow quantification of **detectability** to be carried out over the entire depth range imaged; thus, it is important that the **low-echo spheres** exist up to the entire scanning window. A phantom limited to a flat scanning surface is acceptable for a linear array, phased array or a flat 2-D array but not for the remaining types of arrays. Each of the phantoms specified in this document contains a random distribution of equal diameter [2], **low-echo spheres** existing at all depths, including the case of those designed for testing convex (curved) arrays.

This document summarizes the requirements for a phantom to provide for determination of **detectability** of small, **low-echo spheres** for any type of pulse-echo transducer, except (perhaps) a 2-D array with a spherical-cap surface.

The International Electrotechnical Commission (IEC) draws attention to the fact that it is claimed that compliance with this document may involve the use of a patent. IEC takes no position concerning the evidence, validity, and scope of this patent right.

The holder of this patent right has assured IEC that s/he/it is willing to negotiate licences under reasonable and non-discriminatory terms and conditions with applicants throughout the world. In this respect, the statement of the holder of this patent right is registered with IEC. Information can be obtained from the patent database available at patents.iec.ch.

Attention is drawn to the possibility that some of the elements of this document may be the subject of patent rights other than those in the patent database. IEC shall not be held responsible for identifying any or all such patent rights.

ULTRASONICS – PULSE-ECHO SCANNERS – LOW-ECHO SPHERE PHANTOMS AND METHOD FOR PERFORMANCE TESTING OF GREY-SCALE MEDICAL ULTRASOUND SCANNERS APPLICABLE TO A BROAD RANGE OF TRANSDUCER TYPES

1 Scope

This document, which is a Technical Specification, defines terms and specifies methods for quantifying detailed imaging performance of real-time, ultrasound B-mode scanners. Detail is assessed by imaging phantoms containing small, low-echo spherical targets in a tissue-mimicking background and analysing sphere **detectability** [3]. Specifications are given for phantom properties. In addition, procedures are described for acquiring images, conducting qualitative analysis of sphere **detectability**, and carrying out quantitative analysis by detecting sphere locations and computing their contrast-to-noise ratios. With appropriate choices in design, results can be applied, for example:

- to assess the relative ability of scanner configurations (scanner make and model, scan head and console settings) to delineate the boundary of a tumour or identify specific features of tumours;
- to choose scanner control settings, such as frequency or the number and location of transmit foci, which maximize spatial resolution;
- to detect defects in probes causing enhanced sidelobes and spurious echoes.

The types of transducers used (see sections 7.6 and 10.7 of [1]) with these scanners include:

a) phased arrays,
b) linear arrays,
c) convex arrays,
d) mechanical sector scanners,
e) 3-D probes operating in 2-D imaging mode, and
f) 3-D probes operating in 3-D imaging mode for a limited number of sets of reconstructed 2-D images.

The test methodology is applicable for transducers operating in the 1 MHz to 23 MHz frequency range.

2 Normative references

The following documents are referred to in the text in such a way that some or all of their content constitutes requirements of this document. For dated references, only the edition cited applies. For undated references, the latest edition of the referenced document (including any amendments) applies.

IEC 60050-802, *International Electrotechnical Vocabulary – Ultrasonics* (available at: http://www.electropedia.org)

IEC 61391-1, *Ultrasonics – Pulse-echo scanners – Part 1: Techniques for calibrating spatial measurement systems and measurement of system point-spread function response*

IEC 61391-2:2010, *Ultrasonics – Pulse-echo scanners – Part 2: Measurement of maximum depth of penetration and local dynamic range*

IEC TS 62736, *Ultrasonics – Pulse-echo scanners – Simple methods for periodic testing to verify stability of an imaging system's elementary performance*

3 Terms and definitions

For the purposes of this document, the terms and definitions given in IEC 60050-802, IEC 61391-1, IEC 61391-2 and the following apply.

ISO and IEC maintain terminological databases for use in standardization at the following addresses:

- IEC Electropedia: available at https://www.electropedia.org/
- ISO Online browsing platform: available at https://www.iso.org/obp

3.1
active area of a transducer
area over which transducer transmitting and/or receiving elements are distributed

3.2
backscatter coefficient
intrinsic backscatter coefficient
η
intrinsic property of a material, at some frequency, equal to the differential scattering cross-section per unit volume for a scattering angle of 180°

Note 1 to entry: See [4], [5], [6].

[SOURCE: IEC 61391-1:2006, 3.6, modified – The term "differential scattering cross-section" is used in place of factors comprising this quantity that are included in the source definition.]

3.3
low-echo sphere
hypoechoic sphere
spherical inclusion in a phantom, with a **backscatter coefficient** that is lower than the **backscatter coefficient** of the surrounding tissue-mimicking material

3.3.1
low-constrast, low-echo sphere
low-echo sphere with a **backscatter coefficient** that is 6 dB (±0,2 dB) lower than the **backscatter coefficient** of the surrounding tissue-mimicking material

3.3.2
high-contrast, low-echo sphere
low-echo sphere with with a **backscatter coefficient** that is at least 30 dB lower than the **backscatter coefficient** of the surrounding tissue-mimicking material

Note 1 to entry: See also 6.3.

3.4
sphere diameter
D
diameter of spherical inclusions in a phantom

Note 1 to entry: It is generally assumed that all **low-echo spheres** in a particular phantom have the same diameter D.

3.5
pixel
smallest spatial unit or cell size of a digitized two-dimensional array representation of an image

Note 1 to entry: Each **pixel** has an address corresponding to its position in the array.

Note 2 to entry: **Pixel** is a contraction of "picture element".

[SOURCE: IEC 61391-1:2006, 3.23, modified – Supplementary information has been moved from the definition to Note 1 to entry; the words "and a specific brightness level" have been deleted from the supplementary information.]

3.6
pixel value
integer value of a processed signal level or integer values of processed colour levels, provided to the display for a given pixel

Note 1 to entry: In a grey-scale display the pixel value is converted to a luminance by some, usually monotonic, function. The set of integer values representing the grey scale runs from 0 (black) to $(2^M - 1)$ (white), where M is a positive integer, commonly called the bit depth. Thus, if M = 8, the largest **pixel value** in the set is 255.

3.7
digitized image data
two-dimensional set of **pixel values** derived from the ultrasound echo signals that form an ultrasound image

3.8
mean pixel value
MPV
mean of **pixel values** detected over a designated area or volume in an image or 3D stack of images. For low echo spheres here, MPV is defined for an area A in a phantom image, where A is somewhat smaller than the area of a circle of diameter D

Note 1 to entry: The phrase "somewhat smaller than" is introduced as partial compensation for the partial volume effect in the elevational dimension [3].

Note 2 to entry: The partial volume effect is a term common in computed tomography, magnetic resonance imaging, and ultrasound imaging. This process refers to the effect of the finite imaging resolution, particularly the slice thickness. The signal (pixel values) at points near the object boundaries will include contributions from that object and contributions from the material around it. For example, if the object is a sphere with diameter close to the thickness of the slice, then one cannot define a good measurement region in the image of the sphere in which the signal does not include components from material lying outside the sphere.

3.9
depth interval
interval between boundaries of contiguous depth segments into which an image area is subdivided for computation of $LSNR_{md}$-values as a function of depth

Note 1 to entry: A rectangular scan area will be subdivided into horizontal bands; a sector scan area will be subdivided into annular ring segments, the angular limits being determined by the sector angle (see Figure B.2 d). Rectilinear projection of these area segments in the elevational direction will create volume segments analogous to slabs and partial cylindrical shells, respectively, with thickness equal to the **depth interval extent** Δ.

3.9.1
depth interval label
d
integer for identifying **depth intervals** in an image

Note 1 to entry: d = 1, 2, …, d_{max} where 1 is at the least depth and d_{max} is at the greatest depth.

Note 2 to entry: In computations of the centre of the nth sphere cluster in Annex E, the correct value of d on the right sides of Formulas (E.1), (E.2) and (E.3) depends on the specific i,j coordinates of each site, s, in the cluster. When the cluster extends beyond a boundary of a **depth interval** into an adjacent volume segment, then d will be incremented or decremented by 1 for those sites located in the adjacent volume segment.

3.9.2
depth interval extent
Δ
extent of each equal segment into which an image area is subdivided for computation of $LSNR_m$-values as a function of depth

Note 1 to entry: **Depth interval extent** is expressed in millimetres (mm).

Note 2 to entry: Experience determining $LSNR_m$-values for numerous cases has led to the conclusion that a 4-mm value of Δ is adequate for the phantoms containing 4,0 mm-diameter and 3,2 mm-diameter **low-echo spheres**, and a 2-mm value of Δ is adequate for the phantoms containing 2 mm-diameter **low-echo spheres**.

Note 3 to entry: The maximum image depth is the sum of a set of contiguous **depth interval extents**; thus, if the imaging depth is 16 cm and each **depth interval** spans 4 mm = 0,4 cm, then there are 16/0,4 = 40 **depth intervals**. Equivalently, the maximum image depth is the product of the maximum **depth interval label**, d_{max}, and the **depth interval extent** Δ. The maximum image depth is $d_{max} \times \Delta = 40 \times 0{,}4 = 16$ cm in this example.

3.10
detectability
numerical value quantifying the probability that a human observer will detect an object in an image having background speckle

3.11
lesion signal-to-noise ratio
$LSNR$
ratio of the **mean pixel value** over a region of a detected target in an image, minus the **mean pixel value** over a specified region of the background echo signals, to the standard deviation of the **mean pixel values** contributing to the background

Note 1 to entry: See Formula (2) in 8.4.1 and [7]. Also, see $LSNR_n$ in Clause 4.

3.12
lesion signal-to-noise ratio for the *n*th low-echo sphere
$LSNR_n$
numerical value quantifying the **detectability** of the nth macroscopically uniform, **low-echo sphere** surrounded by a macroscopically uniform, background material and existing in the volume of a phantom for which image data has been obtained

Note 1 to entry: n = 1, 2, 3 ... N_0, where N_0 is the total number of spheres, the centres of which have been approximated.

Note 2 to entry: $LSNR_n$ is a symbol representing $(S_{Ln} - S_{mBn})/\sigma_{Bn}$, where S_{Ln} is the mean pixel value calculated over a designated area centred on the nth detected sphere, S_{mBn} is the mean pixel value from designated areas of the background region not containing spheres and σ_{Bn} is the standard deviation of all MPVs contributing to S_{mBn}. These symbols are defined in Clause 4 and are explained further in 8.4.1.

Note 3 to entry: **Low-echo spheres** with centres located less than a distance $D/2$ from a lateral **image boundary** are excluded.

3.13
mean lesion signal-to-noise ratio
$LSNR_m$
conceptual mean value of the **lesion signal-to-noise ratio** for detected **low-echo spheres** whose centres lie within an unspecified volume segment

3.14
$LSNR_{md}$
mean lesion signal-to-noise ratio for **depth interval** d
Mean LSNR
mean lesion signal-to-noise ratio for detected spheres whose centres lie within the volume segment denoted by **depth interval label** d

Note 1 to entry: **Low-echo spheres** with centres located less than a distance $D/2$ from a lateral **image boundary** are excluded.

Note 2 to entry: In figures in several annexes, the ordinate label of the left graph a) is "Mean LSNR"; this label corresponds to $LSNR_{md}$ in accordance with the notation adopted in 8.4.2.

3.15
image plane
plane of symmetry of the acoustic pulses for generating an image on the monitor

3.16
image boundary
boundary of the displayed monitor image

Note 1 to entry: For example, see the rectangular image in Figure B.5.

3.17
image data set
image set
set of data images derived from parallel **image planes** which are separated from adjacent **image planes** by $D/4$

Note 1 to entry: See also Clause 7.

3.18
specific attenuation coefficient
<at a specified frequency> attenuation coefficient divided by the frequency

[SOURCE: IEC 61391-2:2010, 3.33, modified – The source definition – "at a specified frequency, the slope of attenuation coefficient plotted against frequency" – has been rephrased.]

3.19
cubic array
set of sites or positions in three-dimensional σ space with Cartesian coordinates $x = iD/4$, $y = jD/4$ and $z = kD/4$, where $iD/4$ and $jD/4$ lie in an **image plane**, $kD/4$ specifies a particular **image plane** and i, j and k are integers

Note 1 to entry: Since all Cartesian coordinates have a common factor of $D/4$, the convention is adopted that i, j or k without the $D/4$ factor are taken to mean the Cartesian coordinates $iD/4$, $jD/4$ or $kD/4$. Also, ijk means the **cubic array** site with coordinates $iD/4$, $jD/4$ and $kD/4$.

Note 2 to entry: The smallest volume describable with these **cubic array** sites is a cube of volume $(D/4)^3$

4 Symbols

Symbol	Meaning	Reference
A	square area in an **image plane** selected for calculation of MPV	3.8, 8.2
η_{obj} η_{bkg}	**backscatter coefficient** of an embedded object and of background material, respectively	3.2
D	**low-echo sphere diameter**	3.4
d	integer for identifying **depth intervals**	3.9, 8.4.2 E.1
d_{min}	integral number of the **depth interval** chosen as the minimum depth for applying the data analysis; minimum depth = $d_{min}\Delta$	8.3.2
d_{max}	greatest integral number of the **depth intervals** allowed by the chosen maximum possible depth for data analysis; maximum depth = $d_{max}\Delta$	8.3.1, Annex E
i, j, k	integers corresponding to rows (i) and columns (j) and the elevational position (k) of a **cubic array**, respectively	3.9 (see Note 1) 8.2
$LSNR_m$	conceptual **mean lesion signal-to-noise ratio**	3.13, 8.4
$LSNR_{md}$	**mean lesion signal-to-noise ratio** for detected spheres whose centres lie within the volume segment denoted by **depth interval label** d NOTE The term "Mean LSNR" is used as ordinate labels on data figures in Annex B, Annex C, Annex G, Annex H and Annex I.	3.14, 8.4 8.1
$LSNR_n$	**lesion signal-to-noise ratio for the nth low-echo sphere,** calculated using $LSNR_n = \frac{(S_{Ln} - S_{mBn})}{\sigma_{Bn}}$ where the meanings of the terms are listed below in this table	3.12, 8.4.1
$LSNR_{n,d}$	**lesion signal-to-noise ratio for the nth low-echo sphere** in the volume segment denoted by **depth interval label** d	3.11, 8.4.1
M_d	mean of all MPVs with centres lying within the volume denoted by **depth interval label** d, using the entire image set	Annex E
$M_{d(ij)n,s}$	M_d designation in Formulas (E.1), (E.2), and (E.3) in Annex E, where the **depth interval**, d, for specific index values, s, in the summation will vary, depending on the cubic-array coordinates, ij, of individual sites in the nth cluster. Label d varies, depending on how close the detected cluster is to a **depth interval** boundary, causing individual sites comprising the cluster to lie in different **depth intervals**. d also depends on whether the transducer is a linear array, convex array or phased array. NOTE For linear arrays, d has no j-dependence.	Annex E
MPV	**mean pixel value**	3.8, 8.2
$(MPV)_{ijk}$	MPV calculated over an area A centred at the ijk-site of the **cubic array**	3.19, (see Note 1), 8.2
$(MPV)_n = S_{Ln}$	MPV calculated over area A centred at the projection of (x_{CMn}, y_{CMn}) onto the **image plane** nearest to z_{CMn}	8.2
N_o	total number of detected **low-echo spheres** with centres in the volume equal to the area surrounded by the **image boundary** multiplied by the distance between the first and the last **image planes**, and excluding any spheres situated less than $D/2$ from the boundary of that volume	3.12
N_d or N,d (as required by software)	number of detected **low-echo spheres** comprising N_o that have centres within the volume segment denoted by **depth interval label** d	8.4.2
n	integer for identifying clusters of neighbouring $(MPV)_{ijk}$ sites that differ from the background **pixel value** by at least 1,5 standard deviations	3.12 Annex E
n_d or n,d (as required by software)	integer-subscript for identifying subsets of $(MPV)_{ijk}$ site clusters, whose computed centres lie within the **depth interval** denoted by label d	8.4.2

Symbol	Meaning	Reference
$P(u)$	probability of there being u **low-echo sphere** centres in an arbitrarily chosen 1-ml volume	6.2.4
q	exponent of the frequency dependence of the **backscatter coefficient**	6.3
r (in Annex F)	index, taking values 1 or 2 to indicate one side or opposite side of a phantom, wherein a reflector is situated	Formula (F.1)
R_i and N_i	**mean pixel values** on the reflector side and non-reflector side of a phantom, respectively (see Figure F.1)	Formula (F.1)
$S_{Ln} = (MPV)_n$	MPV calculated over area A centred at the projection of (x_{CMn}, y_{CMn}) onto the **image plane** nearest to z_{CMn}	8.4.1
S_{mBn}	mean of all MPVs in the specified **image plane,** whose centres are within the annulus defined by radii equal to $(3/4)D$ and $2D$ and centred at the coordinates of S_{Ln}	8.4.1
σ_d	standard deviation of all $(MPV)_n$'s with centres lying within the volume segment corresponding to **depth interval label**, d, using the entire image set	Annex E
t_n or t,n (as required by software)	number of sites in a detected MPV cluster	Annex E
Δ	interval in depth of contiguous area segments into which an image area is subdivided for computation of $LSNR_{md}$-values as a function of depth	3.9
x_{CMn}, y_{CMn}, z_{CMn}	coordinates of the "centre of mass" of the nth **low-echo sphere**	8.4.1, 8.4.2, Annex E
v	mean number of **low-echo sphere** centres per millilitre; or volumetric concentration of **low-echo sphere** centres	6.2.4
σ_{Bn}	standard deviation of all MPVs contributing to S_{mBn}	8.4.1
z_{ip}	z-coordinate of points in an **image plane**	8.2

NOTE Additional symbols used only in relation to Annex E or Figure F.4 are defined in the text in Annex E and below Figure F.4.

5 General and environmental conditions

The manufacturer's specification should allow comparison with the results obtained from the tests defined in this document.

All measurements should be performed within the following ambient conditions:

– temperature, 23 °C ± 3 °C;

– relative humidity, 10 % to 95 %;

– atmospheric pressure, 66 kPa to 106 kPa.

Properties of ultrasound phantoms, such as speed of sound and attenuation coefficient, can vary with temperature. Consult the specifications published by the phantom manufacturer to determine whether the expected acoustic properties are maintained under the above environmental conditions. If not, the environmental conditions over which expected and reproducible results can be obtained from the phantom or test object should be adopted for tests specified below.

6 Equipment required

6.1 General

The test procedures specified in this document should be carried out using B-mode images of tissue-mimicking phantoms containing **low-echo spheres**. Analysis should be done on **digitized image data** acquired from the ultrasound scanner. A range of sphere diameters and contrasts, as in contrast-detail analysis, would provide comprehensive information on **detectability** of low-contrast lesions and, indirectly, discrimination of tumour border features; however, full coverage of the contrast-detail space would require many phantoms and spherical targets. Therefore, two phantoms, each having a specified target contrast and each with one of two sphere sizes, are chosen here to give a cost-effective method of testing ultrasound systems.

For phantoms used for assessing and intercomparing the ability of imaging systems to delineate tumour boundaries, a tight tolerance on the sphere size is necessary. The properties of these phantoms are specified in 6.2.1. The tolerance of sphere diameters is loosened somewhat in 6.2.2 for phantoms used to evaluate overall scanner performance, tune scanner pre-sets, and detect transducer defects. This loosening is expected to enable more widespread availability and frequent use of these systems by clinical facilities.

6.2 Phantom geometries

6.2.1 Low-contrast phantoms for assessing the ability to delineate tumour boundaries

6.2.1.1 For use in the frequency range 1 MHz to 7 MHz

The phantom should allow imaging to a depth of at least 8 cm and provide for display of the entire B-scan image frame. **Low-contrast, low-echo spheres** (**backscatter coefficient** −6 dB (±0,2 dB) relative to that of the background material in the phantom) should be available for **detectability** assessment over the entire image frame. The diameter of these spheres should be specified by the manufacturer to within ±2 %. The mean number of spheres per unit volume should be at least one per millilitre but the volume fraction consisting of spheres should not exceed 3,3 %. Scanning windows should provide for contact of the entire emitting surface of the transducer (**active area of a transducer**), while allowing elevational translation of the transducer over a sufficient distance that the most likely number of spheres traversed by the scan plane at or near the focal distance(s) is 40 or more in a 5 mm-**depth interval**. A low-echo **sphere diameter** of 3,2 mm is recommended for adequate performance assessment in the 1 MHz to 7 MHz range.

NOTE 1 One **low-echo sphere** can serve as two such spheres, if total internal reflection at a planar surface provides an independent image. See Annex A for an example of the geometry.

NOTE 2 The **detectability** of −6 dB spheres has replaced **detectability** of −20 dB spheres in IEC TS 62791:2015, regarding delineation of the boundary of a tumour. Superiority of **detectability** (more negative **detectability**) of one scanner configuration over another for −20 dB spheres will likely apply at all spherical-object contrasts; however, −6 dB is much closer than −20 dB to the range of contrasts needed.

6.2.1.2 For use in the frequency range 7 MHz to 23 MHz including "micro-convex" arrays

The phantom should allow imaging to a depth of at least 4 cm and provide for display of the entire B-scan image frame. **Low-contrast, low-echo spheres** (**backscatter coefficient** −6 dB (±0,2 dB) relative to the backscatter coefficiemt of the background material) should be available for **detectability** assessment over the entire image frame, and the diameter of these spheres should be specified by the manufacturer to within ±2 %. The mean number of spheres per unit volume should be at least eight per millilitre but the volume fraction consisting of such spheres should not exceed 3,3 %. A low-echo **sphere diameter** of 2 mm is recommended for adequate performance assessment in the 7 MHz to 23 MHz range. Scanning windows should provide for contact of the entire emitting surface of the transducer, while allowing elevational translation of the transducer over a sufficient distance that the most likely number of spheres traversed by the scan plane at or near the focal distance(s) is 40 or more for a **depth interval extent** of 2 mm.

NOTE One **low-echo sphere** can serve as two such spheres, if total internal reflection of a beam at a planar surface provides an independent image. See Figure D.1 for an example of the geometry.

6.2.2 High-contrast phantoms to evaluate scanner performance, tune scanner pre-sets, and detect defects in probes

6.2.2.1 For use in the 1 MHz to 7 MHz frequency range

The phantom should allow imaging to a depth of at least 18 cm and provide for display of the entire B-scan image frame. **High-contrast**, **low-echo spheres** (**backscatter coefficient** at least 30 dB lower than the **backscatter coefficient** of the background material, unless otherwise specified) should be available for **detectability** assessment over the entire image frame. A low-echo **sphere diameter** of 4 mm or 6 mm is recommended for adequate performance assessment in the 1 MHz to 7 MHz range. Larger diameters are useful for testing low frequency systems that image to depths greater than 30 cm. The diameter of these spheres should be specified by the manufacturer to within ±0,2 mm. The mean number of spheres per unit volume should be at least one per millilitre but the volume fraction consisting of spheres should not exceed 0,15 (15 %). Scanning windows should provide for contact of the entire emitting surface of the transducer.

NOTE If larger spheres (> 5 mm diameter) are used, the 0,15 volume fraction limit could require less than one sphere per millilitre.

6.2.2.2 For use in the 7 MHz to 23 MHz frequency range, including "micro-convex" arrays

The phantom should allow imaging to a depth of at least 8 cm and provide for display of the entire B-scan image frame. High-contrast, **low-echo spheres** (**backscatter coefficient** at least 30 dB lower than the backscatter coefficient of the background material in the phantom, unless otherwise specified) should be available for **detectability** assessment over the entire image frame. A low-echo **sphere diameter** of 2 mm ± 0,2 mm is recommended for adequate performance assessment in the 7 MHz to 23 MHz range, and the diameter of these spheres should be specified by the manufacturer to within ±9 %. The mean number of spheres per unit volume should be at least eight per millilitre but the volume fraction consisting of such spheres should not exceed 15 %. Scanning windows should provide for contact of the entire emitting surface of the transducer.

NOTE High-contrast (−20 dB and −40 dB) spheres are expected to be detectable over a greater depth range than the low-contrast (−6 dB) spherical targets in 6.2.1. Consequently, the phantom depth range is greater in 6.2.2 than in 6.2.1.

6.2.3 Total internal reflection surfaces

Total internal reflection surfaces can be used to reduce the phantom lateral dimensions and conserve numbers of **low-echo spheres** needed for fabrication. For phantoms with **low-echo spheres** having diameters of 3 mm to 4 mm, two parallel, plate-glass surfaces causing total internal reflection are acceptable in the phantom, as shown in Figure A.1 and Figure A.2. For phantoms with **low-echo spheres** having diameters of 2 mm, two parallel, planar, alumina surfaces causing total internal reflection are acceptable in the phantom, as shown in Figure D.1; a surface roughness of the alumina of 6 µm or less is sufficient.

6.2.4 Spatially random distribution of low-echo spheres

Though the positioning of **low-echo spheres** in the phantom can be precisely defined, manufacturing costs will likely be much lower, if the spheres are spatially randomly distributed.

The spatially random distribution of **low-echo spheres** in a phantom is closely approximated by the Poisson probability distribution function,

$$P(u) = \frac{e^{-v} v^{u}}{u!} \tag{1}$$

where

e is Euler's Number (2,718 28....) and the base of natural logarithms;

v is the mean number of **low-echo sphere** centres per millilitre.

For example, if v = 1 and $P(u)$ is the probability of there being u **low-echo sphere** centres in an arbitrarily chosen 1-ml volume, the standard deviation is $\sigma = v^{1/2} = 1$.

6.3 Ultrasonic properties of the tissue-mimicking (TM) phantoms

For any phantom, the following ultrasonic property ranges are specified to apply at 23 °C.

NOTE Property values and tolerances specified here are generally similar, but not identical, to those specified in IEC 61391-1:2006 and IEC 61391-2:2010.

Mass density: 0,95 g ml^{-1} to 1,15 g ml^{-1}. To minimize or to avoid detection of specular reflections from sphere boundaries, the background and sphere materials should have the same acoustic impedance to within 1 %.

Specific attenuation coefficient: (0,50 ± 0,04) dB cm^{-1} MHz^{-1} at 3 MHz, or some more appropriate value for the background material (surrounding the **low-echo spheres**) and the value for the **low-echo sphere** material should be within 0,04 dB cm^{-1} MHz^{-1} of the background value.

Propagation speed: (1 540 ± 10) m s^{-1}. For phantoms designed for specific applications of body parts with speed of sound clearly different than 1 540 m s^{-1}, materials with that speed of sound may be used. In that case, the phantoms shall be labelled clearly as intended for that application with a "nonstandard speed of sound" of (the intended speed) ± 10 m s^{-1}.

Backscatter coefficient for the 1 MHz to 23 MHz frequency range:

For the background material: 3 × 10^{-4} (sr cm)$^{-1}$ ± 3 dB at 3 MHz and frequency dependence of (frequency)^{q}, where 3 ≤ q ≤ 4.

For the low-contrast sphere material: No lower (more negative) than −6,2 dB, and no greater than −5,8 dB relative to the background material.

For the high-contrast sphere material: No higher than −40 dB with respect to the **backscatter coefficient** of the background material, unless otherwise specified.

Long-term stability: With appropriate attention, a phantom should maintain its original values of **backscatter coefficient** within ±5 dB, **specific attenuation coefficient** within ±8 %, propagation speed ±1 % and density ±2 % for at least 5 years. For water-based tissue-mimicking materials this requirement can be assured by periodic monitoring of a phantom's weight as specified by the manufacturer. When the weight has decreased by a specified amount, the phantom can be returned to the manufacturer for transfusion with sufficient aqueous solution to return the phantom to its weight (and presumably ultrasonic properties) at the time of manufacture.

7 Data acquisition assuming a spatially random distribution of low-echo spheres

7.1 Methodology

7.1.1 General

The basic unit for data acquisition for transducer types a) through d) of Clause 1 is a digitized grey-scale image including the entire selected field of view. Typically, at least 8 bits (256 levels) of distinct grey levels are realized. For transducer types e) and f) of Clause 1, see Annex J. For each transducer tested, ultrasound system controls including the field of view, ultrasound frequency, transmit focus settings (if available), output power setting, overall gain, time gain compensation (TGC), and pre- and post-processing settings should be recorded. One way to accomplish this recording is to develop a system preset that stores the above settings once an optimized image of the phantom has been generated over the usable depth range for that transducer. This "**low-echo sphere**" preset should be stored in the scanner's preset menu listings for each transducer, and it should be available for future tests of the probe or of similar probes. Alternatively, a clinical preset that is applicable to an anatomical site commonly scanned using the transducer may be selected, though the system performance might not be optimized for imaging this phantom. This preset should be noted for future tests.

NOTE It is customary that software and hardware will be made available which simplify acquisition, recording and long-term storage of these data.

The TGC can be difficult to reproduce unless it is set with all depth ranges at maximum or minimum settings, or at an easily identified centre position. These positions usually do not yield the best results obtainable with these measurements, but are recommended. The measurements can be highly dependent on modest changes in the TGC. Usually, the manual TGC is not among the controls included in the presets.

Figure 1 shows a flow chart of the methodology.

7.1.2 Mechanical translation

The measurement protocol involves acquiring images while the transducer under test is translated in the elevational direction over a section of the specified phantom. For those systems in which the beam axes corresponding to the image frame lie in a plane (defining the "scan plane"), the transducer should be held in contact with a section of the scanning window (with adequate coupling gel) by an apparatus which also allows translation in the elevational direction, thereby allowing acquisition of image frames with scan planes parallel to one another [7], [8].

NOTE Either the transducer or the phantom can be translated.

The translational increment between acquired frames is a function of the low-echo **sphere diameter** and allows the plane of symmetry (scan plane) of at least one frame to lie within 1/8 of the sphere diameter from the centre of a detected sphere; i.e. the maximum increment should be equal to 1/4 of the sphere diameter.

7.1.3 Manual translation with cine-loop recording

Manual translation of the transducer, while images are recorded in the form of a cine loop, also is possible with many ultrasound systems. This method of data acquisition can also be carried out, if shown to be equivalent to the case of images recorded in conjunction with mechanical translation. When recording a cine loop, the transducer shall be translated perpendicularly to the scan acquisition plane, translation shall be at a uniform speed, and the distance between the **image planes** recorded on individual cine frames shall be known. For a uniform translation speed, the distance equals the total translation distance for which the cine loop was recorded divided by (the number of image frames contained in the loop minus 1). Just as in the case of mechanical translation, the interframe distance should be no greater than 1/4 of the sphere diameter.

NOTE If an alternative method for determination of **low-echo sphere** centres were shown in a peer-reviewed publication to be at least as accurate as the method in Clause 7 and Annex E, and alternative software were also made available for computing $LSNR_m$-values as a function of depth, which agree to within +10 % with values obtained in [7], [8], then employment of such an alternative method would not be in conflict with this document.

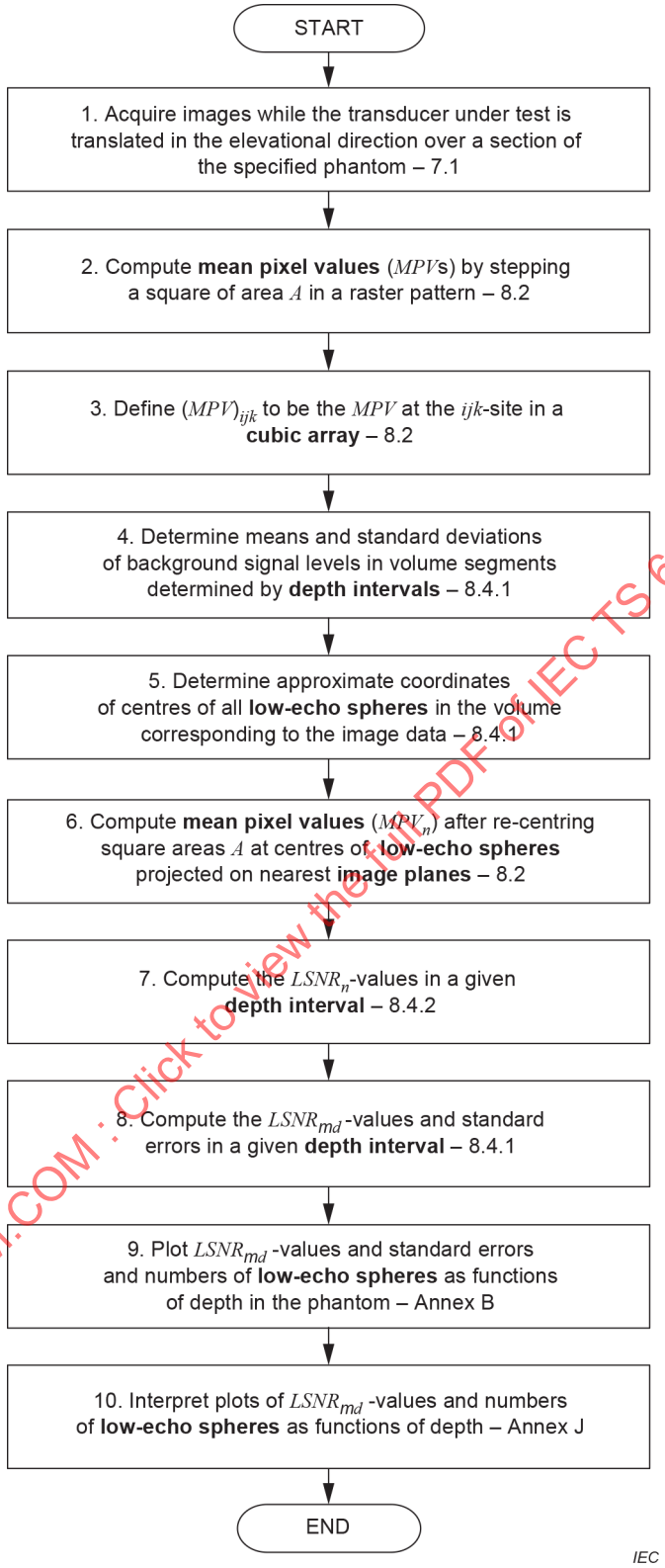

Figure 1 – Flow chart

7.2 Storage of digitized image data

Image data are available on most scanners in a DICOM (Digital Imaging and Communications in Medicine [9]) format. Software capable of transferring and opening DICOM-formatted images is available. When bitmap images are available from the scanner, those also can be used. Factors outlined in 6.4 of IEC 61391-2:2010 apply.

7.3 Digital image files available from the scanner itself

This method is used by most scanner manufacturers for in-house quality-control testing and image-processing development. Capabilities exist to extend the method for use by clinical personnel using, for example, file-transfer protocol (ftp) resources. Alternatively, many scanners provide image files on removable media, such as USB thumb drives, magneto-optical disks, zip disks, or CD-ROM, and these are appropriate sources of digital image data as well. Full-screen capture is available on many systems.

7.4 Image archiving systems

Many imaging centres use commercially available Picture Archiving and Communication Systems (PACS) for storing and viewing ultrasound image data. Manufacturers of PACS systems usually provide means to acquire images in an uncompressed format, such as a 'tiff' (Tagged Image File Format) or a DICOM [9] format, by workstations that have access rights to the image data.

8 Automated data analysis for quantifying low-echo sphere detectability

8.1 General

Using the image data obtained as specified in Clause 7 and assuming negligible gradients in background MPVs, the human-observer-related **detectability** equals the **mean lesion signal-to-noise ratio** ($LSNR_{\mathrm{m}}$) in each one of contiguous volume segments determined by the **depth intervals** spanning the entire depth range available [3], [7], [8].

Recall from 3.12 that the **lesion signal-to-noise ratio for the *n*th low-echo sphere** ($LSNR_n$) is a numerical value quantifying the **detectability** of a macroscopically uniform, **low-echo sphere** in a macroscopically uniform, surrounding-background material [10]. Each **depth interval** contains a subset of the N_{o} centres. **Low-echo spheres** and background material have **intrinsic backscatter coefficients**, namely, η_{obj} and η_{bkg}, respectively. For a spherical inclusion, $LSNR_n$ has been defined and discussed extensively [11].

8.2 Computation of mean pixel values (*MPV*s)

MPV, as defined in 3.8, is the mean of **pixel values** detected over an area A in a phantom image, where A is somewhat smaller than the area of a circle of diameter D; this definition allows for partial compensation for the partial volume effect in the elevational dimension [3].

In this document, A is a square with side $2D/3$ [3]. For each image obtained in accordance with 7.1, a set of MPVs is computed over areas A, stepped in a raster pattern in the **image plane**, with centres comprising a simple, square array and nearest neighbour spacing of $D/4$. Thus, for all images obtained by translating the transducer under test in the elevational direction in successive steps of $D/4$, each MPV in a set is associated with one of the sites in a simple, **cubic array**.

Define $(MPV)_{ijk}$ to be the MPV at the ijk-site, where i, j and k are integers and $(D/4)i$ is the x-coordinate value, $(D/4)j$ is the y-coordinate value, and $(D/4)k$ is the z-coordinate value of the site. Also, i corresponds to rows, j to columns, and k to the elevational direction, of the **cubic array**.

Next, the coordinates (x_{CMn}, y_{CMn}, z_{CMn}) of the centres of **low-echo spheres** should be determined (see first paragraph in 8.3.1 and Annex E). The spheres are labelled 1, 2, 3 … N_o. Then, for each n, the **mean pixel value** in the **image plane** nearest to the nth **low-echo sphere** centre for the site having x- and y-coordinates equal to those of the centre (x_{CMn} and y_{CMn}) is computed, giving rise to a new set of MPV-values (MPV_n), also designated as S_{Ln} when computing lesion signal-to-noise ratios in Formula (2) below. In general, these x- and y-coordinates will not coincide with the coordinates of any $(MPV)_{ijk}$. MPV_n is computed over a square of area A. (See Figure 2.)

Figure 2 is a schematic of an **image plane** closest to the **low-echo sphere** centre, containing three concentric circles (inner, middle and outer) of radii defined in the key below the diagram of Figure 2, and examples of stepping square areas A, delineated for computing **mean pixel values** $(MPV)_{ijk}$ that are assigned to the array sites (▪) centred in each square.

MPVs assigned to image-plane sites in the central cross-hatched area are excluded from calculations of the background means and standard deviations, while MPVs assigned to image-plane sites in the diagonally hatched area are included, unless they are within a sphere of radius $3D/4$ concentric with a different **low-echo sphere** centre (e.g. at lower right) or are restricted by linear-array or sector-scan image boundaries. (See Figure 3 to Figure 6 and 8.3.)

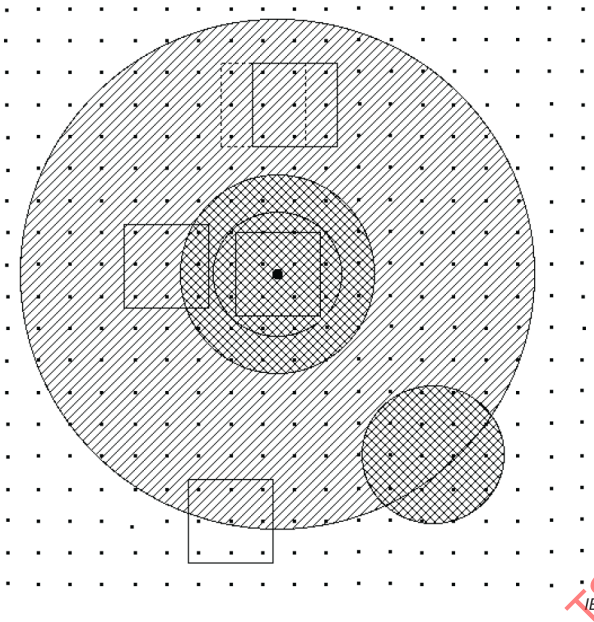

Key

- ▪ (MPV)-array sites (i,j,k) in the **image plane** with grid-spacing $D/4$ – 8.2
- ● Point in the **image plane** nearest to the nth **low-echo sphere** centre having coordinates x_{CMn}, y_{CMn}, z_{ip}, where $| z_{ip} - z_{CMn} | \leq D/8$ and z_{ip} is the z-coordinate of points in the **image plane**.

The inner circle is a **low-echo sphere** boundary (physical) projected onto the **image plane** nearest to the nth **low-echo sphere** centre and centred at ●. Its radius is $D/2$.

The middle circle (mathematical) in the **image plane** has radius $3D/4$ and is centred at ● – see 8.3.1.

The outer circle (mathematical) in the **image plane** has radius $2D$ and is centred at ● – see 8.3.2.

The full-line squares (examples) denote areas A in the **image plane**, having sides of length $2D/3$ and used to compute $(MPV)_{ijk}$ values that are assigned to the array sites (▪) at the centres of those squares – see 8.2.

The dashed-line square (top) denotes the area A in the **image plane** (for computing MPV_{i-1jk}) prior to computing $(MPV)_{ijk}$ – see 8.2.

The full-line square in the centre denotes area A in the **image plane** for computing MPV_n.

The circular cross-hatched area (lower right) has radius ≤ $3D/4$ and denotes the intersected area of the **image plane** with the sphere of radius $3D/4$ (mathematical) centred at another **low-echo sphere**, having its centre at $z \neq z_{CMn}$ – see 8.3.1.

Figure 2 – Schematic of the image plane nearest to the nth low-echo sphere and not influenced by the presence of an image boundary

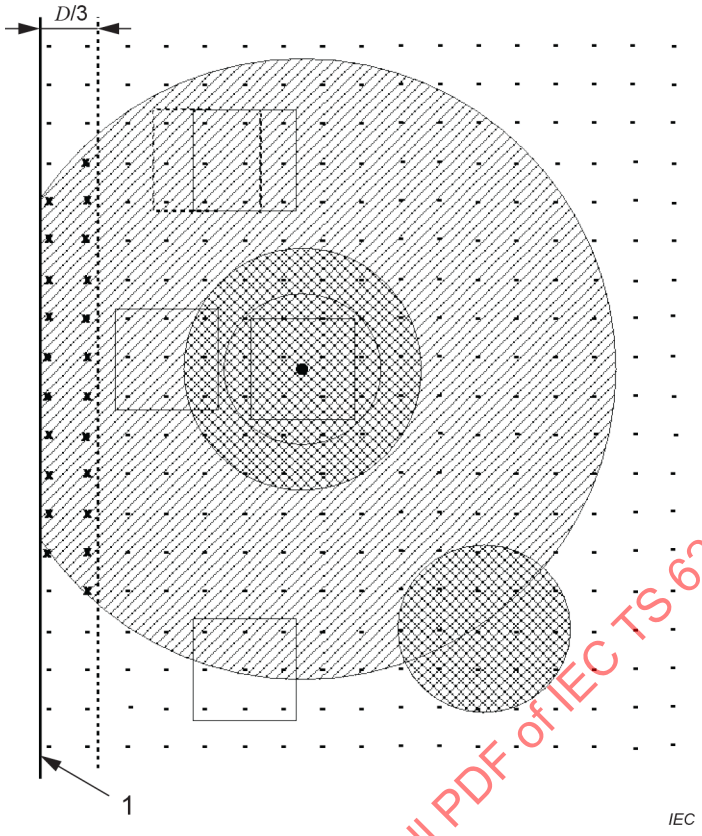

Key

1 vertical **image boundary**

D sphere diameter

The excluded $(MPV)_{ijk}$ values are those corresponding to the x's.

Figure 3 – Modification of Figure 2 showing a vertical image boundary (solid line) and a parallel dashed line, between which $(MPV)_{ijk}$ values are excluded from computation of $S_{\mathrm{mB}n}$ or $\sigma_{\mathrm{B}n}$ in Formula (2)

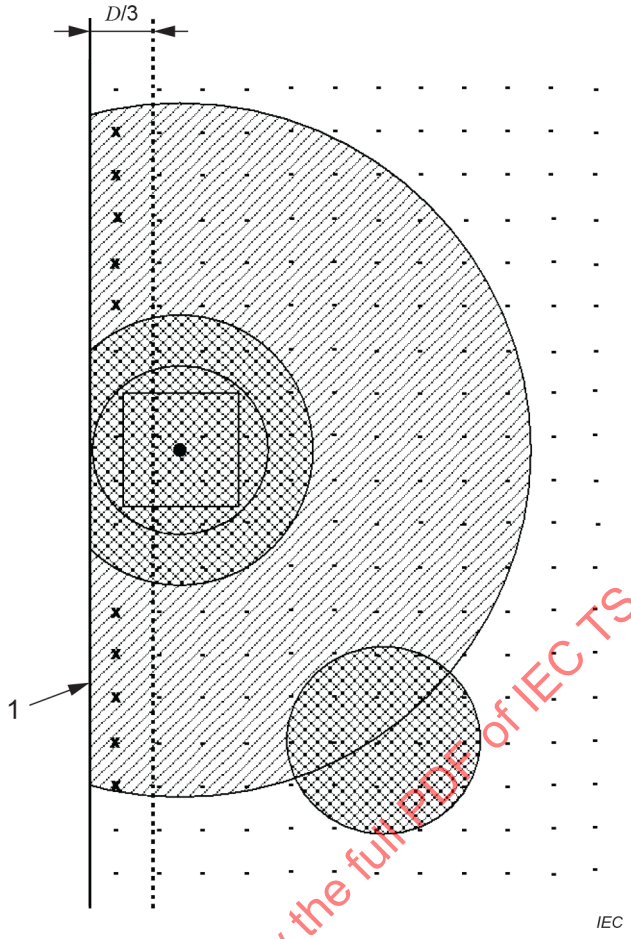

Key

1 vertical **image boundary**

D sphere diameter

The only square area A depicted is that corresponding to the **low-echo sphere** centre.

Figure 4 – Limiting case of Figure 3 where the vertical image boundary is tangent to the imaged low-echo sphere

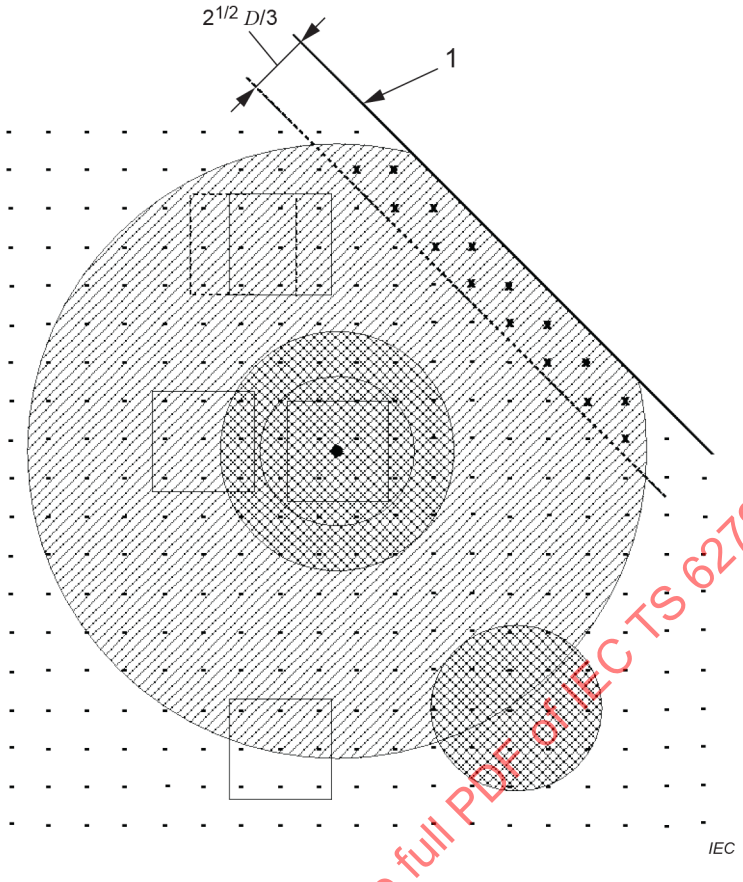

Key

1 slanted **image boundary**

D sphere diameter

The excluded $(MPV)_{ijk}$ values are those corresponding to the x's. For other boundaries with angles between 0 and 45°, corresponding diagrams apply.

Figure 5 – Modification of Figure 2 showing a 45° sector image boundary (solid line) and a parallel dashed line, between which $(MPV)_{ijk}$ values are excluded from computation of $S_{\mathrm{mB}n}$ or $\sigma_{\mathrm{B}n}$ in Formula (2)

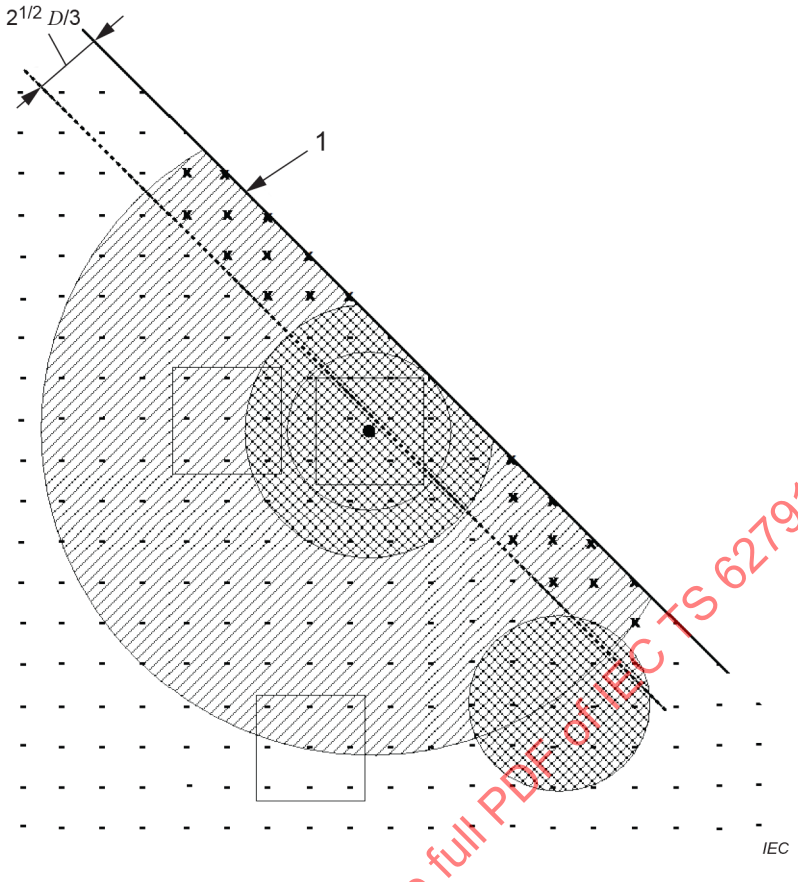

Key

1 slanted **image boundary**

D sphere diameter

$(MPV)_{ijk}$ values at the x's are not included in the computation of S_{mBn} or σ_{Bn} in Formula (2).

Figure 6 – Limiting case of Figure 5 where the 45° sector image boundary is tangent to the imaged low-echo sphere

8.3 Additional restrictions for sector images

8.3.1 Convex arrays

Mean pixel values $(MPV)_{ijk}$ assigned to **cubic array** sites (▪) within $D/2$ of the arc-shaped **image boundary** at zero depth or within $D/2$ of the maximum depth for data analysis should not be used in computations of S_{mBn} or σ_{Bn}. The person operating the software code first specifies a **depth interval** and a maximum possible depth for data analysis after which the software sets the maximum depth for data analysis to be the greatest number, d_{max}, of **depth intervals** allowed by the chosen maximum possible depth.

Also, **mean pixel values** $(MPV)_{ijk}$ assigned to **cubic array** sites (▪) within $D/3$ of vertical bars, selected by the operator of the data analysis code to eliminate echoes due to vertical phantom walls from the image, should not be used in computations of S_{mBn} or σ_{Bn}.

8.3.2 Phased arrays

Generally, zero depth in the displayed phased array image is at the vertex of the sector angle of that displayed image. It is recommended that, after specifying a **depth interval extent**, the operator of the code choose an integral number d_{min}, of **depth intervals** as the minimum depth for applying the data analysis; for example, the minimum depth might approximate the width of the phased array. An arc-shaped boundary will then be defined, and **mean pixel values** $(MPV)_{ijk}$ assigned to **cubic array** sites (▪) within $D/2$ of that arc-shaped boundary should not be used in computations of $S_{\text{mB}n}$ or $\sigma_{\text{B}n}$.

Regarding other exclusions of **mean pixel values** $(MPV)_{ijk}$ assigned to **cubic array** sites (▪), see 8.3.1 for text involving the maximum depth for data analysis and vertical bars selected by the operator of the data analysis code to eliminate from the image the echoes due to vertical phantom walls.

8.4 Determination of the $LSNR_{\text{m}}$-value for a given depth interval

8.4.1 Preliminaries

Firstly, the Cartesian coordinates of the centres of all detectable **low-echo spheres** in the volume segment determined by the **depth interval label** should be determined. A preferred method for accomplishing this is specified in Clause 7 and Annex E; this is also the method used in determining $LSNR_{\text{m}}$-values as a function of depth in other annexes.

Secondly, all MPVs that might be significantly influenced by the presence of a neighbouring **low-echo sphere** should be eliminated for computation of background means and standard deviations in 8.4.2; that is, for this computation, do not use any MPV_{ijk} at **cubic array** sites that lie within a radius equal to $3D/4$ of any **low-echo sphere** centre, the coordinates of which were determined in accordance with the last paragraph above or are restricted by linear-array or sector-scan image boundaries. (See Figure 3 to Figure 6 and 8.4.2).

The $LSNR_n$ for the nth **low-echo sphere** is defined in [7]:

$$LSNR_n = \frac{\left(S_{\text{L}n} - S_{\text{mB}n}\right)}{\sigma_{\text{B}n}} \tag{2}$$

where, in terms of the coordinates of **low-echo sphere** centres as determined in Annex E,

$S_{\text{L}n}$ is an MPV (also called MPV_n) with x- and y-coordinates equal to $x_{\text{CM}n}$ and $y_{\text{CM}n}$, respectively, for the nth sphere and z (elevational) coordinate corresponding to the **image plane** closest to $z_{\text{CM}n}$;

$S_{\text{mB}n}$ is the mean of all MPVs in the specified **image plane** whose centres are within the annulus defined by radii equal to $3D/4$ and $2D$ and centred at the coordinates of $S_{\text{L}n}$ and are subject to limitations involving nearby **low-echo spheres** not having coordinates ($x_{\text{CM}n}$, $y_{\text{CM}n}$, $z_{\text{CM}n}$) (see Figure 2) and/or involving nearby image boundaries (see Figure 3 to Figure 6);

$\sigma_{\text{B}n}$ is the standard deviation of all MPVs contributing to $S_{\text{mB}n}$ [7].

When $LSNR_n$-values are computed from the **low-echo spheres** in volume segment d, the results are designated $LSNR_{n,d}$.

8.4.2 Computation of $LSNR_{md}$ for depth interval label d

The $LSNR_{md}$-value for the volume segment determined by the **depth interval label** d is then

$$LSNR_{md} = \frac{1}{N_d} \sum_{n,d=1}^{N_d} LSNR_{n,d} \tag{3}$$

NOTE The lower bound of summation and subscript of summand would read $n_d = 1$ and n_d, respectively, if software would allow it.

where

n,d's constitute a subset of n's, embracing wherever x_{CMn}, y_{CMn} is a point in the depth interval d, including the entire elevational extent of the **image data set** between the first and last **image planes**. The subset of n,d's does not include sphere centres within $D/2$ of the lateral **image boundary** or within $D/2$ of the first and last **image planes**;

N_d is the total number of detected **low-echo spheres** with centres in the volume segment determined by the **depth interval label** d (including all image frames) but excluding those lying within $2D$ of a phantom boundary.

8.4.3 Standard error corresponding to each $LSNR_{md}$-value

The standard error corresponding to each $LSNR_{md}$-value is given by $N_d^{-1/2}$ times the standard deviation of the $LSNR_{n,d}$-values corresponding to the **depth interval** involved.

9 Visual assessments of images

9.1 Image comparisons

Low-echo sphere phantoms, particularly those containing high-contrast spheres that have **backscatter coefficients** 40 dB lower than the **backscatter coefficient** of the background material, are useful tools to make individual image comparisons, for example, when setting up transmit focal zones and other system pre-sets that affect spatial resolution.

The phantom should be scanned using established and reproducible settings of the ultrasound scanner. Either individual images, or cine loops of image frames acquired during elevational translation of the transducer, as described in 7.1, should be used.

Careful visual analysis is done by way of comparisons of resultant images with the known properties of the sphere phantom. Figure 7 presents example images of a phantom containing 2-mm **low-echo spheres**, scanned using a multirow, 1,25-D linear array transducer. The image on the left was obtained using system pre-sets, including frequency, field of view, gain, dynamic range, and transmit focus positions, which had been optimized for imaging the breast. No echoes should appear in the spherical targets, and these do appear to be clearly visualized down to a depth of approximately 2,5 cm. Although some spheres in the 0 to 2,5 cm zone appear to contain echoes, the random location of the low-echo targets results in any single scan plane intersecting these targets away from their centres, leading to this partial fill-in. Utilizing additional images acquired from uncorrelated scan planes, or viewing a cine loop acquired during transducer translation can help identify these "partial volume" effects. Beyond the 2,5 cm depth, **low-echo spheres** are still seen in the image on the left; however, there appears to be added, scattered echo artifact fill-in of spherical targets, i.e. **low-echo spheres** are not as clearly visualized as at shallower depths.

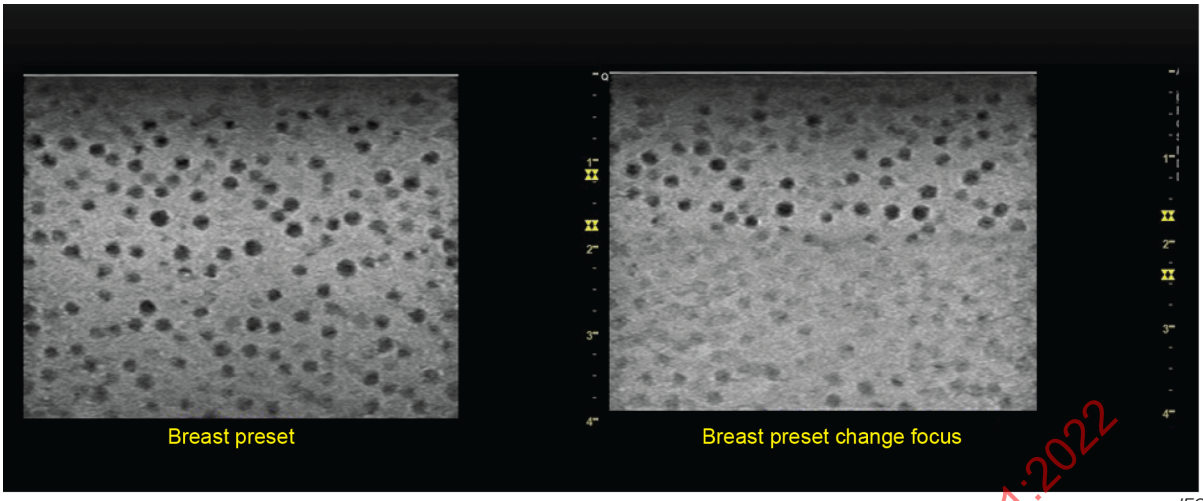

The focal depth-span is indicated on the far right side of each image. The only difference between acquisition parameters of the two images was a slight downward shift of the transmit focal depth of the image on right.

Figure 7 – Usefulness of simple visual inspection of images of a standardized low-echo sphere phantom

One method that might be expected to improve the detail beyond the 2,5 cm depth in Figure 7 (left) image is to increase the depth of the transmit foci positions. These positions are indicated by the hour-glass icons on the right border of each image. In the original image, on the left of Figure 7, the foci are positioned at depths of 1,2 cm and 1,8 cm. The image on the right in Figure 7 illustrates the result of lowering the transmit focal distances to 1,7 cm and 2,4 cm in order to improve visualization of deeper spheres. However, visual inspection of the **low-echo sphere** image on the right of Figure 7 illustrates that in this case, repositioning the transmit foci did not improve the imaging but degraded it.

Inspection of images of standardized **low-echo sphere** phantoms is thus very useful for comparisons of imaging capabilities of different scanner models, optimizing scanner settings for specific imaging tasks, and initial detection of performance deterioration of a scanner or a transducer over a period of time.

More quantitative assessments can be done using the methods in 9.2 or, preferably, using the *LSNR* (**lesion signal-to-noise ratio**) techniques outlined in Clause 8.

9.2 Semi-quantitative image analysis

The following visual analysis can be done using sets of images or preferably using a cine loop acquired during an elevational sweep as described in 7.1. If a cine loop is employed, the cine frames should be displayed at a rate at which the viewer can make estimates of the extent of displayed zones of different clarity. These zones are defined as follows.

Zone 1 ranges are depth ranges, or distances from the transducer, over which at least half of the spheres appear to be clearly outlined as a nearly full-size circle and to be free of echoes.

Zone 2 ranges are depth ranges over which an average of more than one sphere per slice can be discerned.

Examples of the result of this analysis done on the images presented in Figure 7, are shown in Figure 8.

NOTE 1 The images shown in Figure 8 are edited to bring the depth scale and transmit focus icons closer to the corresponding B-mode images, so the source of degradation of the image on the right is seen.

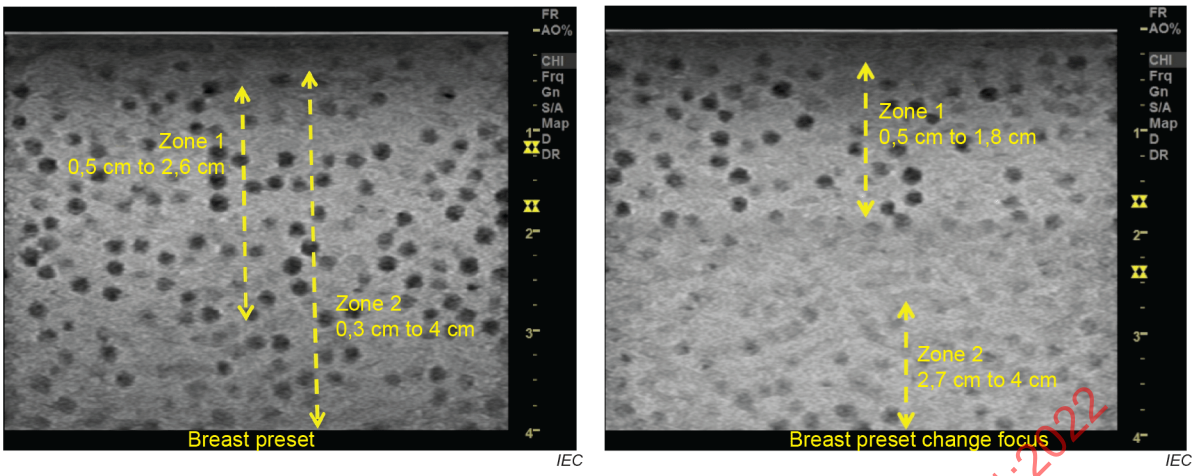

Figure 8 – Zones over which at least half of the spheres appear clearly outlined as a nearly full-size circle and are free of echoes (Zone 1) or an average of more than one sphere per slice can be discerned (Zone 2)

Annex A
(informative)

Example of a phantom for performance testing in the 1 MHz to 7 MHz frequency range

Figure A.1 and Figure A.2 illustrate a phantom containing **low-echo spheres** that meets the specifications in this document.

In Figure A.1 the ends of a conical scanning window for curved arrays are depicted at the top of the phantom. The flat scanning window at the front accommodates linear arrays, phased arrays and flat 2-D arrays [2]. Parallel plate-glass rectangles on the left and right sides provide – via total internal reflection – for extension of the image outside of the volume occupied by tissue-mimicking material.

Dimensions in centimetres

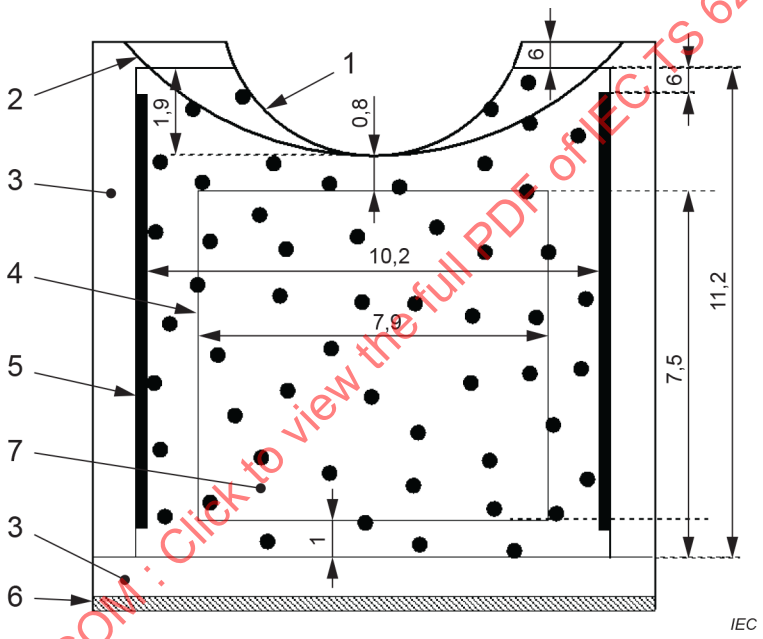

Key

1 3,5-cm-radius-of-curvature scan window at TM material boundary

2 7,5-cm-radius-of-curvature scan window at TM material boundary

3 0,95-cm-thick acrylic wall

4 flat scanning window

5 3-mm-thick plate-glass reflector

6 3-mm-thick cork base

7 background at 1 540 ms^{-1} and 0,5 $dBcm^{-1}$ MHz^{-1} with two 3,2-mm-diameter spheres per millilitre

Figure A.1 – End view of the phantom applicable for 1 MHz to 7 MHz showing the spatially random distribution of 3,2-mm-diameter, −6 dB spheres

Figure A.2 is a top view of the same phantom.

Dimensions in centimetres

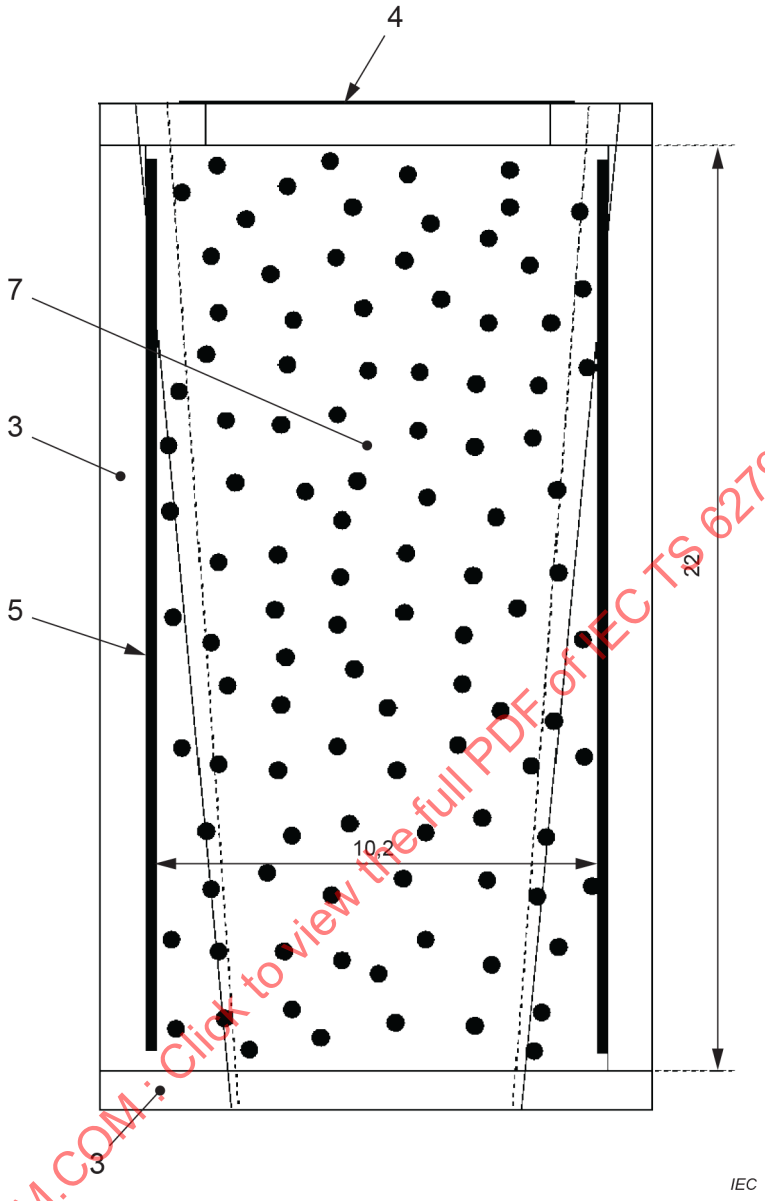

Key

3 0,95-cm-thick acrylic wall

4 flat scanning window

5 3-mm-thick plate-glass reflector

7 background at 1 540 ms^{-1} and 0,5 $dBcm^{-1}$ MHz^{-1} with two 3,2-mm-diameter spheres per millilitre

Figure A.2 – Top view of phantom with 3,2-mm-diameter, −6 dB spheres

Annex B
(informative)

Illustrations of the computation of $LSNR_{md}$-values as a function of depth

Figure B.1 shows an image of a prototype phantom having nearly the same dimensions as those depicted in Figure A.1 and Figure A.2. The phantom contains 4-mm-diameter, −20 dB spheres randomly distributed throughout its volume. A flat alumina reflector exists in place of one of the plate-glass reflectors in Figure A.1. The alumina reflector has a slightly rough surface, giving rise to diffuse echoes at its surface and resulting in the vertical line of elevated echoes on the left. A parallel, 3-mm-thick, plate-glass reflector exists 10 cm to the right of the alumina plate, but no echoes are seen from this smooth, specular surface. The maximum width of the sector image is 18,6 cm. Rigorous testing for the effectiveness of either plate-glass or alumina plates, regarding total internal reflection and the effect of surface diffuse scattering, is presented in Annex F.

A set of fifty images from parallel **image planes** separated by 1 mm was obtained with the convex array transducer translated perpendicular to the **image plane**. Analysis specified in Clause 8 was applied to compute **mean pixel values** (MPVs) over square image regions whose sides are $2D/3$, identify the **image plane** closest to the centre of each detected sphere, and compute its $LSNR$.

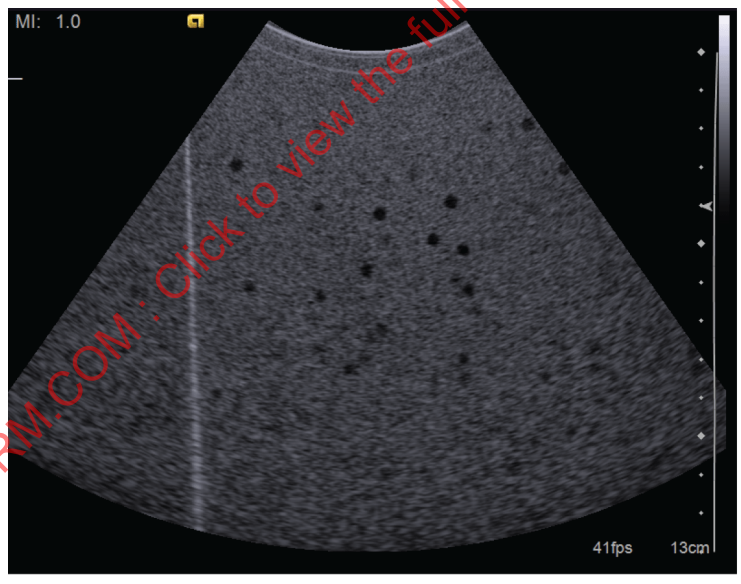

IEC

Figure B.1 – Convex-array image of a prototype 4-mm-diameter, −20 dB sphere phantom for use in the 1 MHz to 7 MHz frequency range

Figure B.2 through Figure B.8 show auxiliary images and results of analysis, as described in more detail in the figure and sub-figure captions. In summary, the 50 images were grouped into two 25-image subsets. "Mean LSNR" ($LSNR_{md}$)-values and standard errors were computed for spheres detected within individual **depth intervals** in each subset, where the **depth interval extent** was 5 mm, yielding plots of Mean LSNR as a function of depth (Figure B.3a). Data from the two subsets show good reproducibility. Then mean $LSNR$ values and standard errors for all 50 images were computed as a function of depth and results plotted for comparison (Figure B.4).

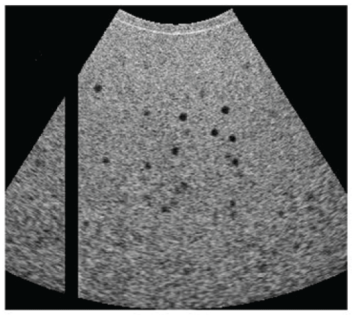

a) Cropped image from Figure B.1 with the vertical line of low-level, diffuse echoes at the flat, alumina plate's surface removed

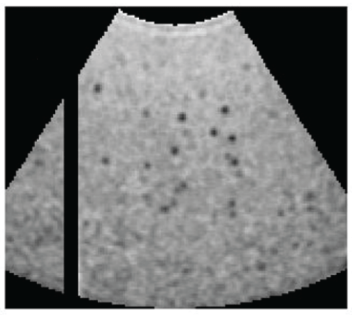

b) Mapping of *MPV*s in grey-scale

c) Sets of 7 sites identified with a −20 dB sphere centre in Figure B.1

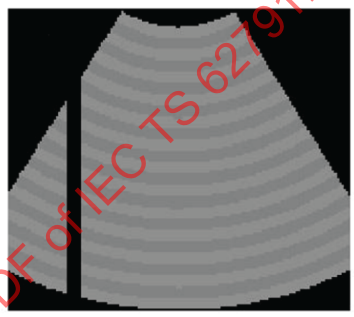

d) 5 mm depth intervals distinguished with different grey levels

Figure B.2 – Auxiliary figures relating to Figure B.1

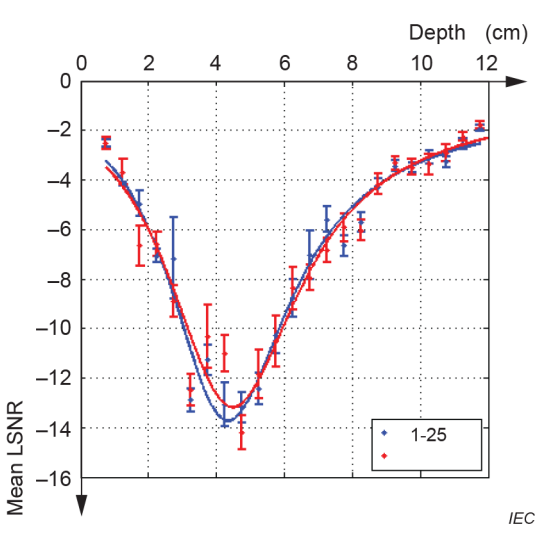

a) Mean LSNR values and standard errors as a function of depth for −20 dB spheres [7], [8], as determined with two independent sets of 25 images corresponding to Figure B.1 and Figure B.2

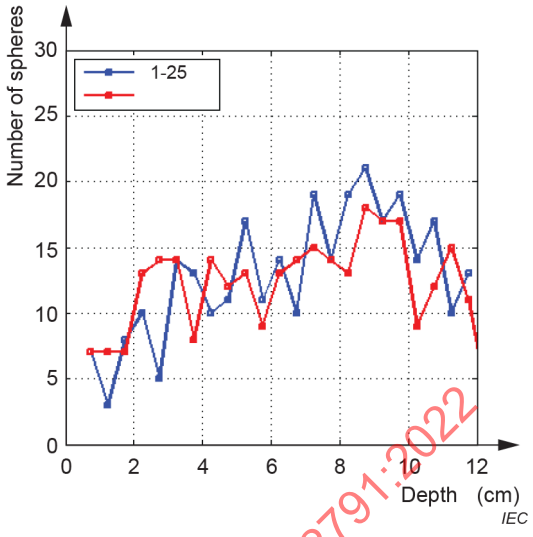

b) Number of −20 dB sphere centres detected in each 5 mm depth interval for the two 25-image sets

NOTE In a), the ordinate label "Mean LSNR" corresponds to $LSNR_{md}$ in accordance with the notation adopted in 8.4.2.

Figure B.3 – Results corresponding to Figure B.1 and Figure B.2, demonstrating reproducibility

In Figure B.4 a) all 50 images are used in one set; such use is recommended. Figure B.4 b) shows that the number of −20 dB spheres in the 5 mm-**depth intervals** in the focal range is about 25.

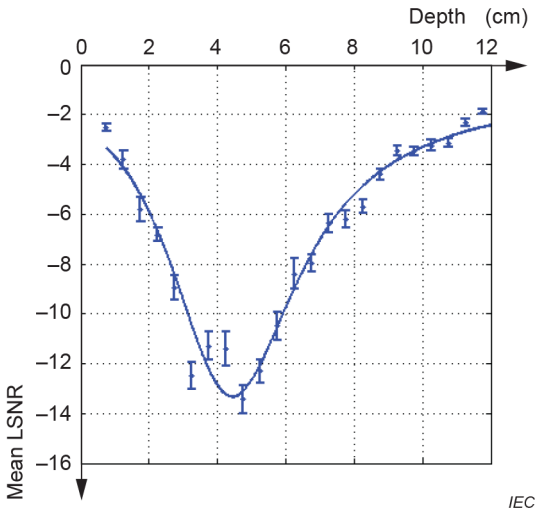

a) **Mean LSNR values as a function of depth for −20 dB spheres [7], [8], using all 50 images corresponding to those in Figure B.3**

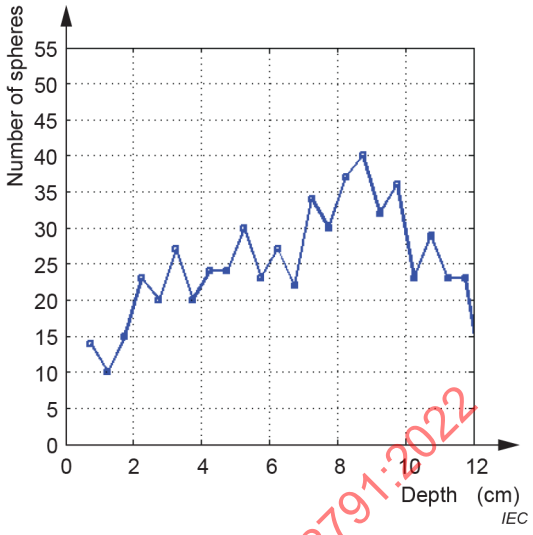

b) **Number of −20 dB sphere centres detected in each 5 mm-depth interval**

NOTE In a), the ordinate label "Mean LSNR" corresponds to $LSNR_{md}$ in accordance with the notation adopted in 8.4.2.

Figure B.4 – Results corresponding to Figure B.1, Figure B.2 and Figure B.3

The evaluation was repeated using a linear-array transducer, generating 80 images in parallel planes, each image plane separated by 1/4 of the sphere diameter, or 1 mm in this case. Figure B.5 is an example of one of the images.

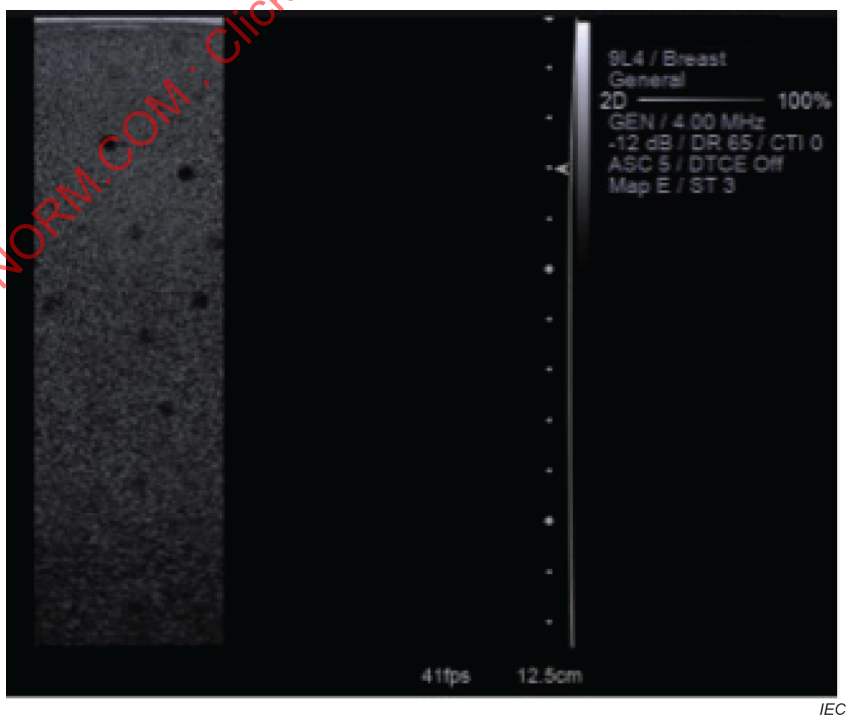

Figure B.5 – One of 80 parallel, linear-array images of the phantom containing 4-mm-diameter, −20 dB spheres, imaged at 4 MHz with the transmit focus at 3 cm depth

In Figure B.6 the image data from this plane (image 18), as well as from the two preceding planes (16, 17), are shown. The green x's indicate the determined centres of the **low-echo spheres** identified with the respective images. On images having partially visualized **low-echo spheres,** where there is no x, the **low-echo sphere** centre was identified in an adjacent **image plane**.

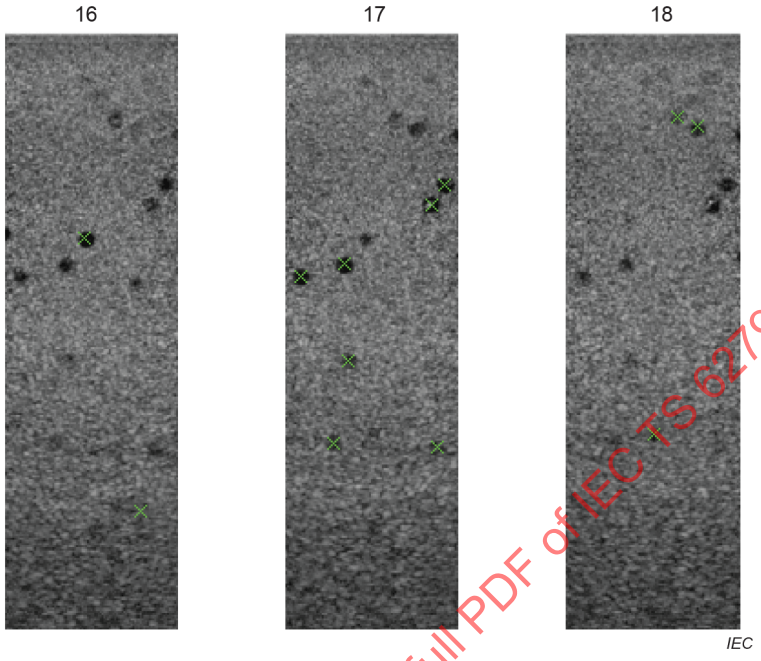

Figure B.6 – Three successive images of the set of 80 frames addressed in Figure B.5, where imaging planes were separated by $D/4$ equal to 1 mm

Analysis of mean $LSNR$s was done by dividing the 80 images into two sets. In Figure B.7 the image set 1 to 40 is independent of the image set 41 to 80. Error bars indicate standard errors. The agreement for the two sets of data plotted in panel a) is reasonable but should be better, if there were more **low-echo spheres** contributing to the mean $LSNR$. Panel b) shows that the mean number of **low-echo spheres** in a depth interval is about 7.

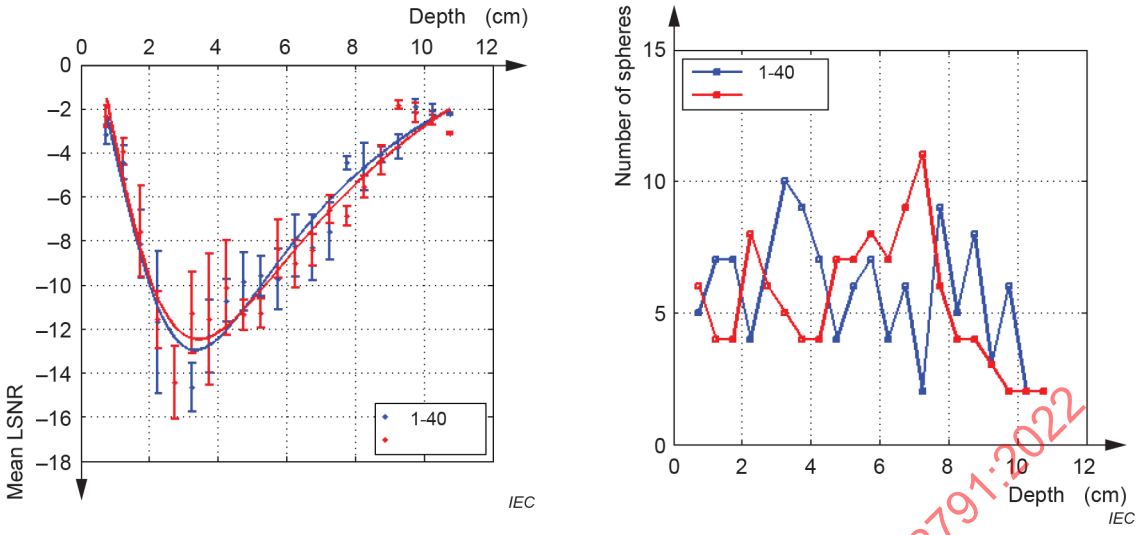

a) Mean LSNR values, along with standard errors as a function of depth for −20 dB spheres [7], [8]

b) Number of −20 dB spheres detected in each 5 mm depth interval

NOTE In a), the ordinate label "Mean LSNR" corresponds to $LSNR_{md}$ in accordance with the notation adopted in 8.4.2.

Figure B.7 – Results for the 4-cm-wide, 3-cm-focus, linear array addressed in Figure B.5 and Figure B.6 using all 80 image frames in two sets

In Figure B.8 a) mean $LSNR$ and standard errors are plotted as a function of depth using the data from all 80 images as a single set. The curve-fit is much better from the doubling of the number of **low-echo spheres** per centimetre **depth interval**. Doubling the number of detected **low-echo spheres** in the 3 cm focal zone would better define the minimum (most negative) value of the mean $LSNR$ ($LSNR_{md}$), but the limited area of the window in this phantom precluded obtaining more than 80 images.

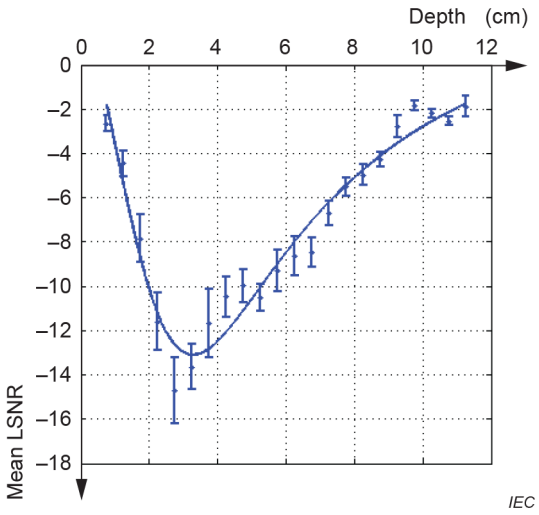

a) **Mean LSNR values as a function of depth for −20 dB spheres [7], [8]**

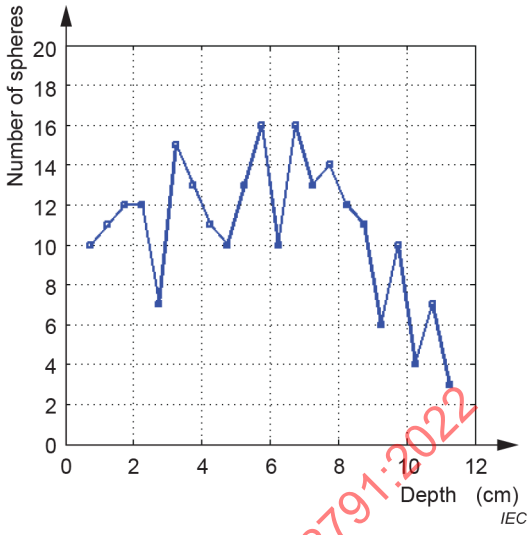

b) **Number of −20 dB spheres detected in each 5 mm depth interval**

NOTE In a), the ordinate label "Mean LSNR" corresponds to $LSNR_{md}$ in accordance with the notation adopted in 8.4.2.

Figure B.8 – Results for the 4-cm-wide, 3-cm-focus, linear array addressed in Figure B.5, Figure B.6 and Figure B.7, using all 80 image frames corresponding to Figure B.7 in one set

Annex C
(informative)

Sufficient number of data images to assure reproducibility of results

C.1 General

In this Annex C evidence is given that the minimum number of data images needed to assure adequate accuracy of $LSNR_{md}$-values is about 25 in the focal zone. Reproducibility using independent (non-overlapping) parts of the phantom is assessed.

C.2 Phantom with 3,2-mm-diameter, −20 dB low-echo sphere, having two spheres per millilitre

The first example is for a linear array operating at 4 MHz with a focus at 3 cm. The elevational interval between images is $D/4$ = 3,2 mm/4 = 0,8 mm. An image is shown in Figure C.1. Results for two cases in which there is no overlap between imaged volumes are shown in Figure C.2. Both sets contain 70 images corresponding to a net elevational displacement of 70 × 0,8 mm = 5,6 cm. Here the mean number of −20 dB sphere centres per 5 mm-**depth interval** is about 15, instead of 25, but reproducibility is still good.

Figure C.1 – One image obtained from a phantom containing 3,2-mm-diameter, −20 dB spheres by using a 4 MHz linear array focused at 3 cm depth

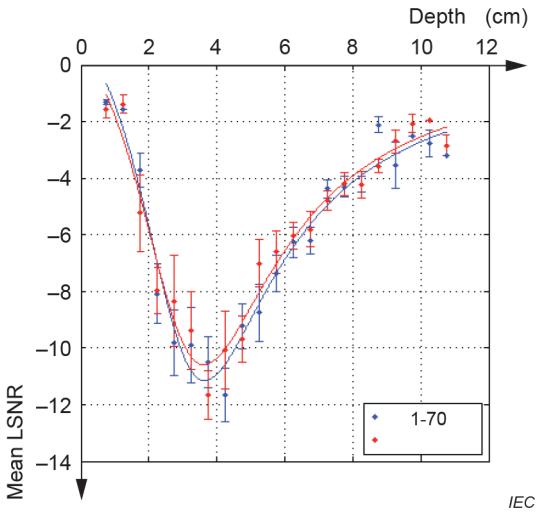

a) **Mean LSNR values as a function of depth for −20 dB spheres [7], [8]**

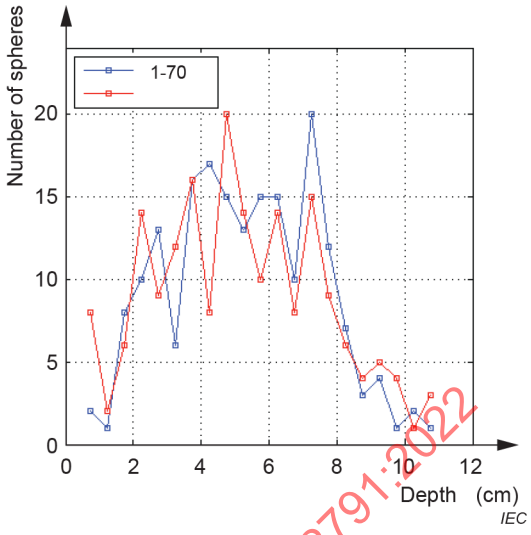

b) **Number of −20 dB sphere centres detected in each 5 mm-depth interval**

NOTE In a), the ordinate label "Mean LSNR" corresponds to $LSNR_{md}$ in accordance with the notation adopted in 8.4.2.

Figure C.2 – Reproducibility result for two independent sets of 70 images with a mean number of low-echo sphere centres that is about 15 per 5 mm-depth interval

Figure C.3 shows the result when the entire 140 images are used and the average number of **low-echo sphere** centres per volume segment determined by the **depth interval** is about 30; the curve fit is excellent indicating excellent reproducibility. The net elevational displacement is 140 × 0,8 mm = 11,2 cm. In Figure C.3 b) the number of **low-echo spheres** per 5 mm-**depth interval** at the focal depth is about 25, corresponding to the recommended number in 6.2.1, and the curve-fit in Figure C.3 a) is good, as expected.

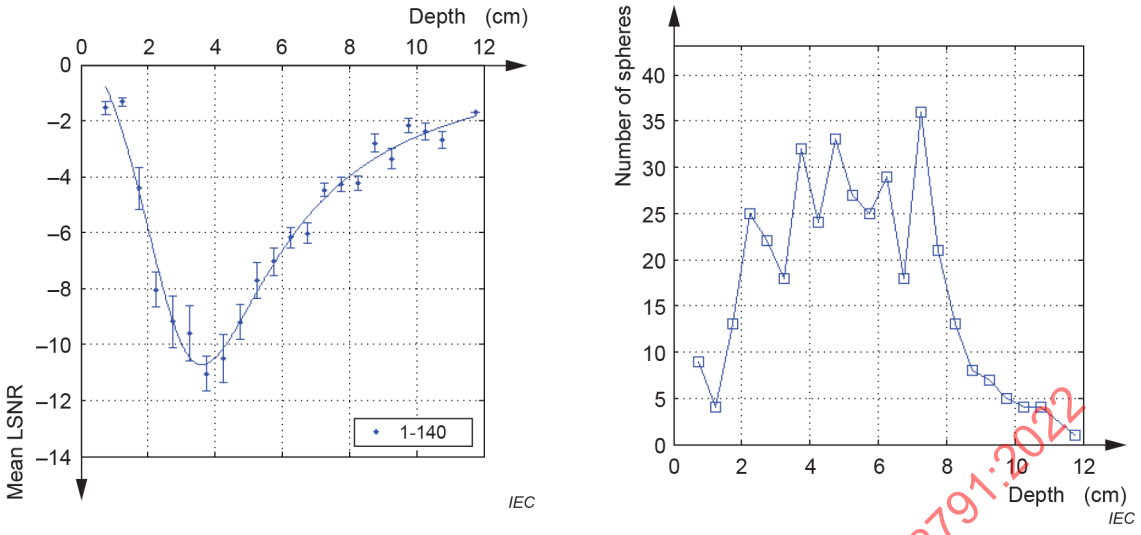

a) Mean LSNR values as a function of depth for −20 dB spheres [7], [8]

b) Number of −20 dB sphere centres detected in each 5 mm-depth interval

NOTE In a), the ordinate label "Mean LSNR" corresponds to $LSNR_{md}$ in accordance with the notation adopted in 8.4.2.

Figure C.3 – Results obtained by combining both sets of 70 independent images corresponding to Figure C.2 into a single, 140-image set

The next reproducibility study involves a convex array operating at 4,5 MHz and illustrates the ability to differentiate performance for different focusing choices. Two sets, each consisting of 50 images separated by $D/4$ = 0,8 mm were obtained for three different transmit focusing conditions. Figure C.4 shows an image with multiple foci at 4 cm, 8 cm and 12 cm; Figure C.5 shows the corresponding reproducibility results. Figure C.6 shows reproducibility results corresponding to a single, deep focus at 10 cm, whereas Figure C.7 corresponds to a single, shallow focus at 4 cm.

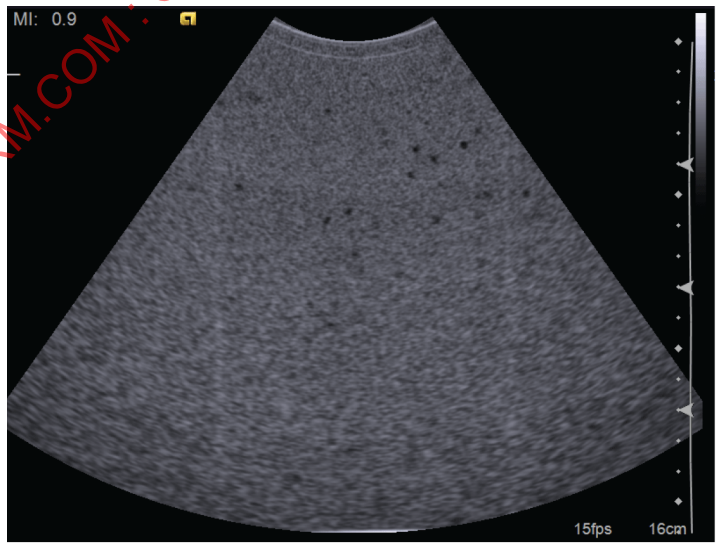

Figure C.4 – Sector image (curved array) at 4,5 MHz with multiple transmit foci at 4 cm, 8 cm and 12 cm depths; the −20 dB spheres are 3,2 mm in diameter

In Figure C.5 a) reproducibility is excellent at a mean number of **low-echo sphere** centres per 5 mm-**depth interval** of 25. The lateral focusing at 8 cm and 12 cm is barely evident, focusing presumably being strongly dominated by fixed elevational focusing at about 4 cm depth.

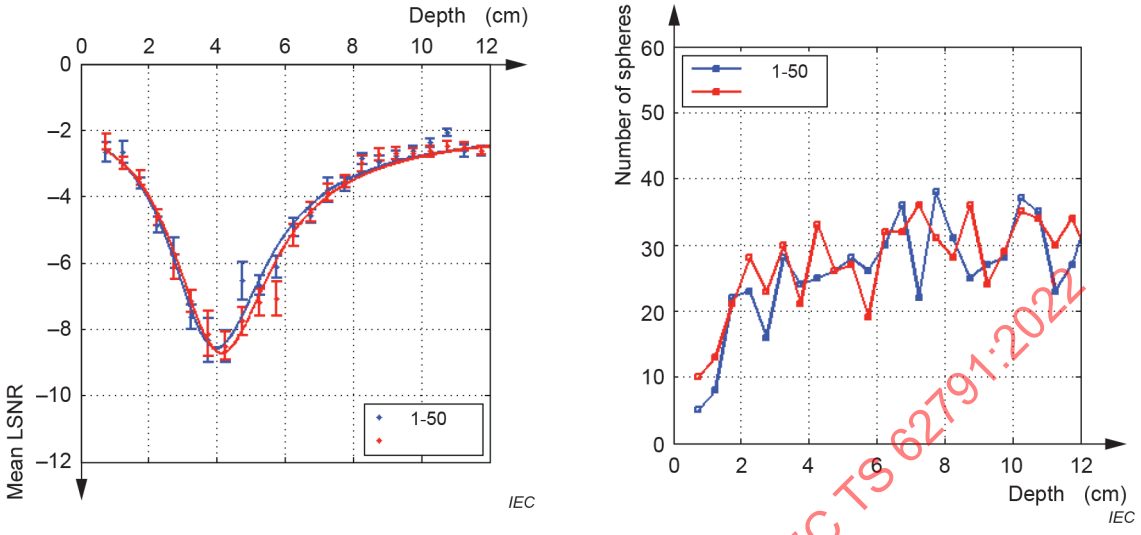

a) Mean LSNR values as a function of depth for −20 dB spheres [7], [8]

b) Number of −20 dB spheres detected in each 5 mm-depth interval

NOTE In a), the ordinate label "Mean LSNR" corresponds to $LSNR_{md}$ in accordance with the notation adopted in 8.4.2.

Figure C.5 – Reproducibility results for a multiple transmit-focus (4 cm, 8 cm and 12 cm) case corresponding to Figure C.4

In Figure C.6 a) reproducibility is excellent at a mean number of **low-echo sphere** centres per 5 mm-**depth interval** of 25. The lateral focusing at 10 cm is not evident, focusing presumably being strongly dominated by fixed elevational focusing at about 4 cm depth. Notice that there is a distinction between these results and the multiple-focus case in Figure C.5, namely a shallower minimum of $LSNR_{md}$ at about −7,9 instead of about −8,7 for the multiple-focus case.

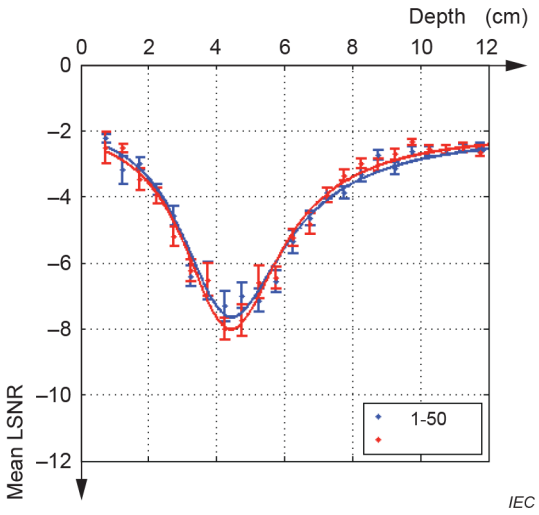

a) **Mean LSNR values as a function of depth for −20 dB spheres [7], [8]**

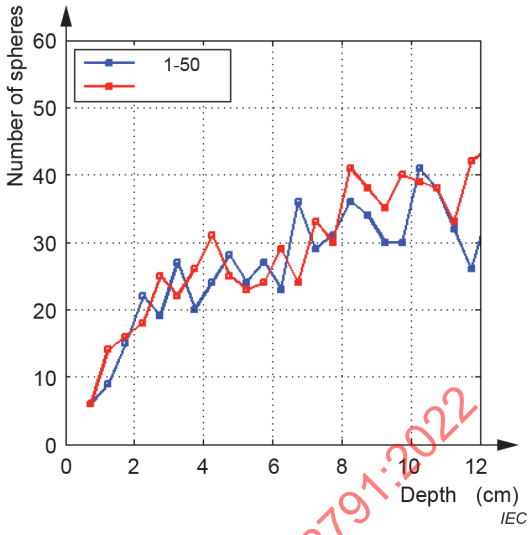

b) **Number of −20 dB sphere centres detected in each 5 mm-depth interval**

NOTE In a), the ordinate label "Mean LSNR" corresponds to $LSNR_{md}$ in accordance with the notation adopted in 8.4.2.

Figure C.6 – Reproducibility results for the case corresponding to Figure C.5, except that there is a single focus at a 10 cm depth

In Figure C.7 a) reproducibility is excellent at a mean number of −20 dB sphere centres per 5 mm-**depth interval** of 25. The 10 cm- and 4 cm-focus cases are almost indistinguishable, the 4 mm case having a slightly deeper minimum (negative value).

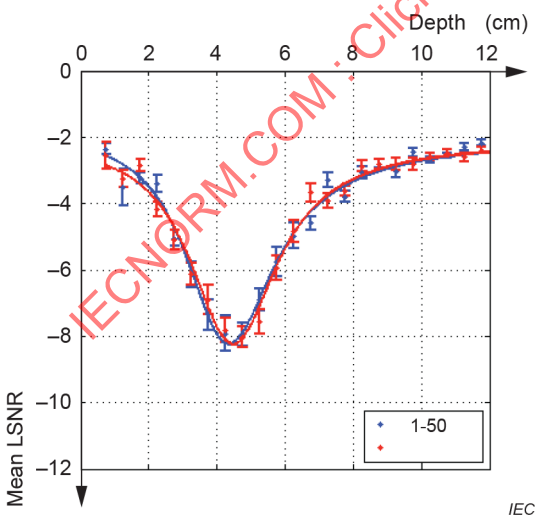

a) **Mean LSNR values as a function of depth for −20 dB spheres [7], [8]**

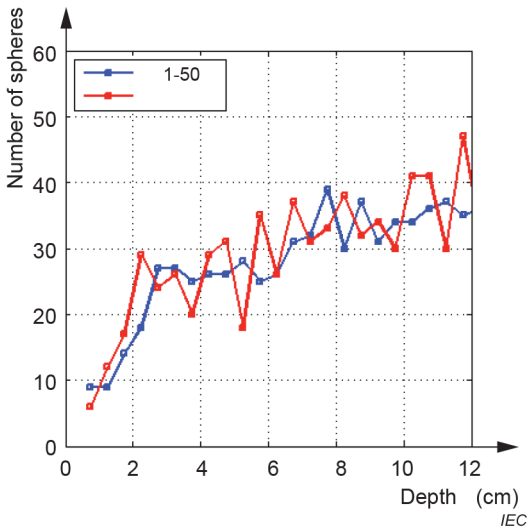

b) **Number of −20 dB sphere centres detected in each 5 mm-depth interval**

NOTE In a), the ordinate label "Mean LSNR" corresponds to $LSNR_{md}$ in accordance with the notation adopted in 8.4.2.

Figure C.7 – Reproducibility results for the case corresponding to Figure C.5, except that there is a single transmit focus at 4 cm depth

C.3 Phantom with 2-mm-diameter, −20 dB spheres and eight spheres per millilitre

Figure C.8 shows an image of a phantom containing 2-mm-diameter, −20 dB **low-echo spheres** and eight spheres per millilitre, made with a curved array having 1,5 cm radius of curvature, with its focus at 3 cm. The C8-5 transducer designation implies that the pulse spectrum lies in the 5 MHz to 8 MHz range.

Figure C.8 – Image of a phantom containing 2-mm-diameter, −20 dB spheres, made with a curved array having a 1,5 cm radius of curvature, with its transmit focus at 3 cm depth

Using this setup, 100 images were obtained in parallel planes separated by $D/4$ = 0,5 mm. Mean $LSNR$-values within 2 mm-**depth intervals** were computed, first for two 50-**image data sets**, then using all 100 images in a single set. Figure C.9 and Figure C.10 show corresponding reproducibility results. (See Annex D for diagrams of this phantom.)

Although $LSNR_{md}$ reproducibility is reasonable in Figure C.9 a), the plotted points are spread more than desired and error bars are rather large. Images 1 to 50 are independent of images 51 to 100. Note from panel b) that the number of **low-echo spheres** detected per 2 mm-**depth interval** in the focal range is about 15, which is fewer than the recommended minimum of 25.

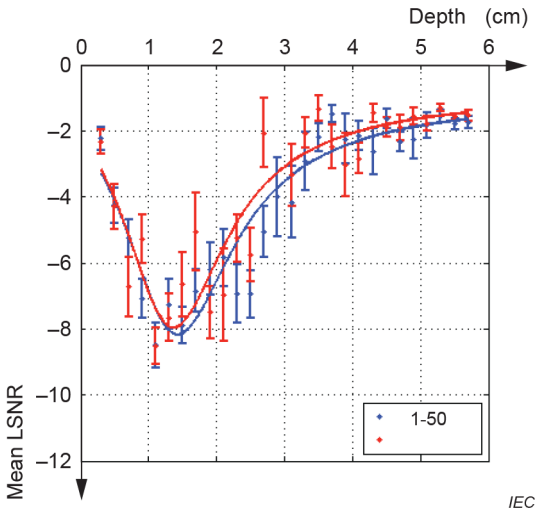

a) Mean LSNR values as a function of depth for −20 dB spheres for each 50-image set [7], [8]

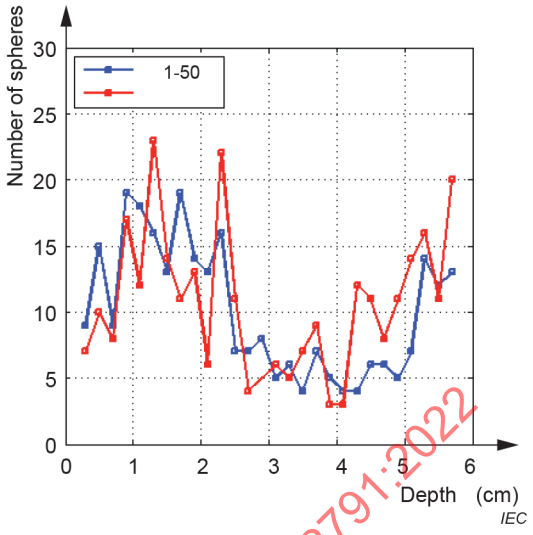

b) Number of −20 dB sphere centres detected in each 2 mm-depth interval for each 50-image set

NOTE In a), the ordinate label "Mean LSNR" corresponds to $LSNR_{md}$ in accordance with the notation adopted in 8.4.2.

Figure C.9 – Reproducibility results corresponding to Figure C.8

In Figure C.10 a) the number of −20 dB **low-echo spheres** per **depth interval** in the focal region (1 cm to 1,5 cm depth range) is about 30 when all images form the data set. The number of detected, **low-echo spheres** per 2 mm-**depth interval** in the depth range 2,5 cm to 3,5 cm is less than 20, compromising the accuracy in that range.

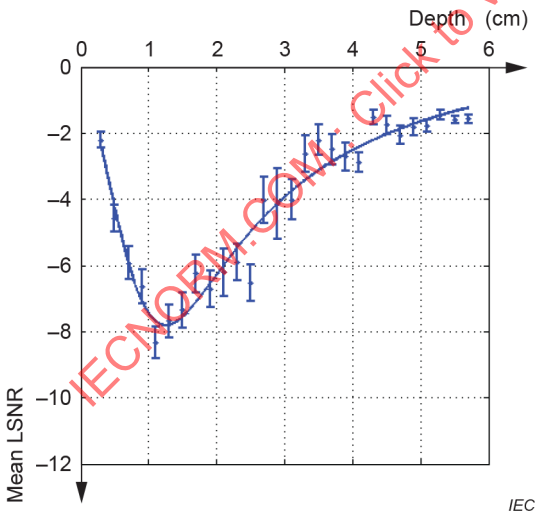

a) Mean LSNR values as a function of depth for −20 dB spheres using all 100 images in the set [7], [8]

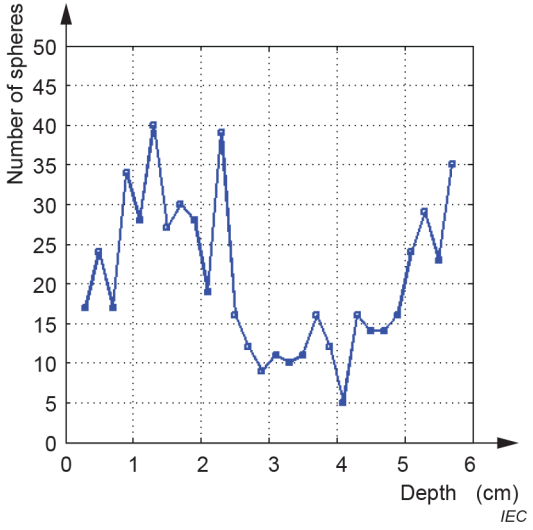

b) Number of −20 dB sphere centres detected in each 2 mm-depth interval

NOTE In a), the ordinate label "Mean LSNR" corresponds to $LSNR_{md}$ in accordance with the notation adopted in 8.4.2.

Figure C.10 – Results using all 100 images in the image set that gave rise to Figure C.9

Figure C.11 shows an image of the phantom containing 2-mm-diameter, −20 dB **low-echo spheres**, made with a high-frequency (15 MHz) linear array, using a transmit focus of 4 cm. 200 images from parallel planes were obtained, with a $D/4$ = 0,5 mm separation between planes. The entire set of images was divided into two 100-image subsets sets for analysis of mean $LSNR$s. Subsequently, all 200 images were analysed as a single set. Figure C.12 and Figure C.13 show corresponding reproducibility results.

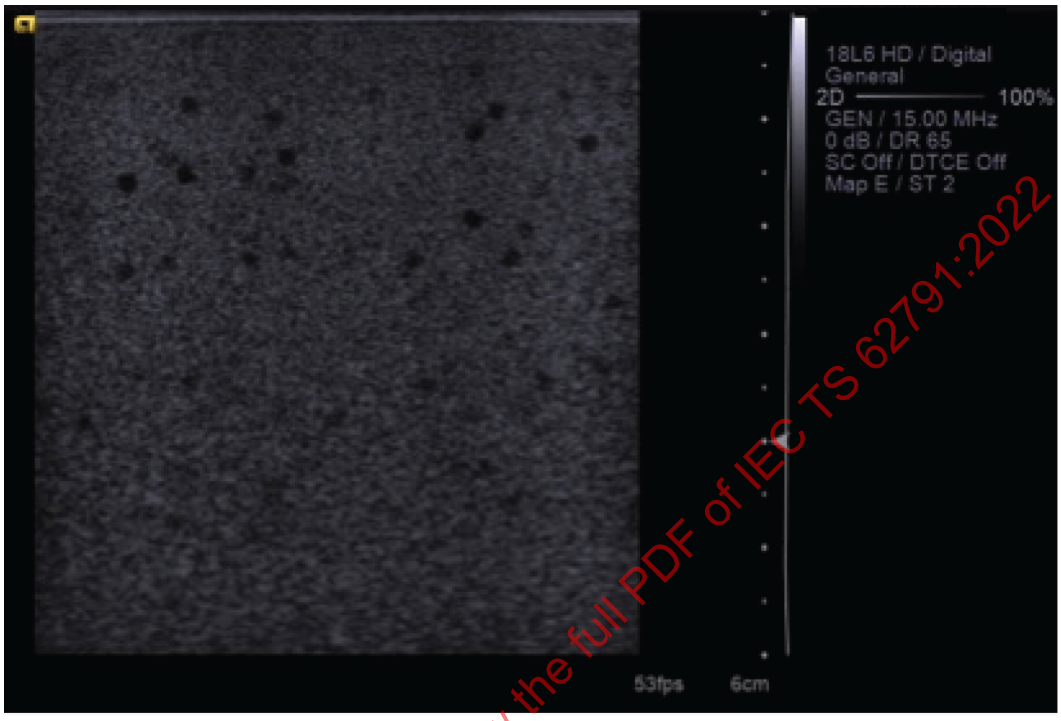

IEC

Figure C.11 – Image of a phantom containing 2-mm-diameter, −20 dB spheres, made with a high-frequency (15 MHz) linear array and a transmit focus of 4 cm depth

In Figure C.12 a) images 1 to 100 are independent of images 101 to 200. Reproducibility is demonstrated with about 35 detected **low-echo spheres** per 2 mm-**depth interval** in the focal-depth range, which again is at the elevational focus of about 1,5 cm.

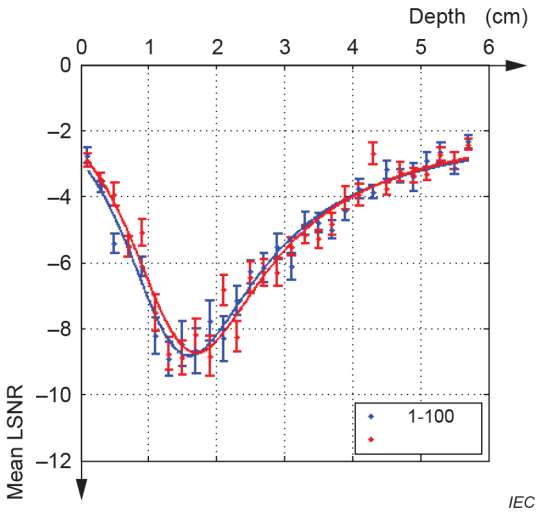

a) **Mean LSNR values as a function of depth for −20 dB spheres for each 100-image subset [7], [8]**

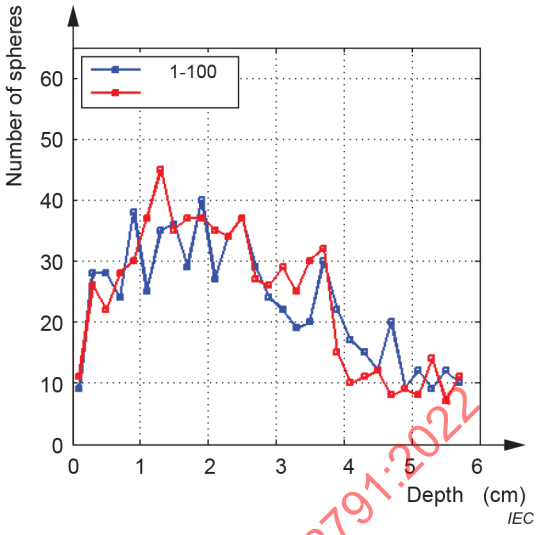

b) **Number of −20 dB sphere centres detected in each 2 mm-depth interval for each subset**

NOTE In a), the ordinate label "Mean LSNR" corresponds to $LSNR_{md}$ in accordance with the notation adopted in 8.4.2.

Figure C.12 – Reproducibility results corresponding to Figure C.11

In Figure C.13 b) using all 200 images to form a set, the number of **low-echo spheres** per 2 mm-**depth interval** in the focal region (1 cm to 1,5 cm depth range) is about 70.

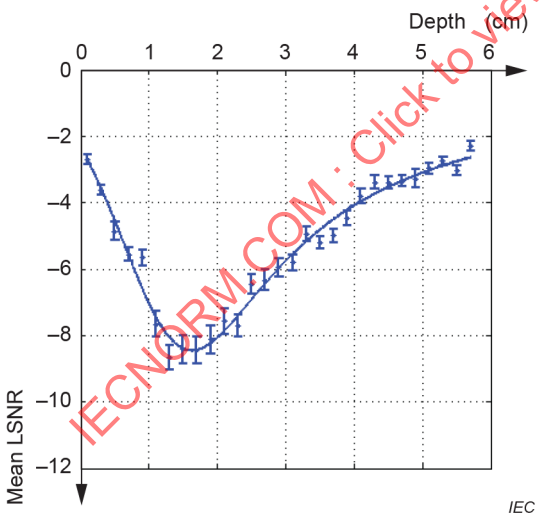

a) **Mean LSNR values as a function of depth for −20 dB spheres [7], [8]**

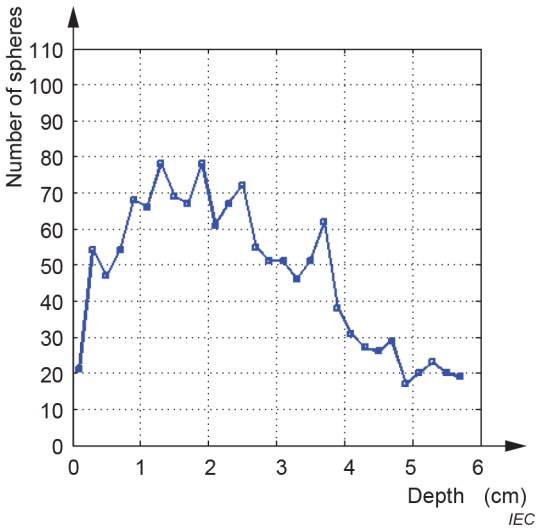

b) **Number of −20 dB spheres detected in each 2 mm-depth interval**

NOTE In a), the ordinate label "Mean LSNR" corresponds to $LSNR_{md}$ in accordance with the notation adopted in 8.4.2.

Figure C.13 – Results using all 200 images in the image set that gave rise to Figure C.12

Annex D
(informative)

Example of a phantom for performance testing in the 7 MHz to 23 MHz frequency range

Figure D.1 illustrates a phantom containing 2 mm, **low-echo** (−20 dB backscatter contrast) **spheres**. Figure D.2 shows an image made with this phantom, in which the −20 dB **low-echo spheres** are clearly visible as black spots without internal reflections.

Dimensions in centimetres

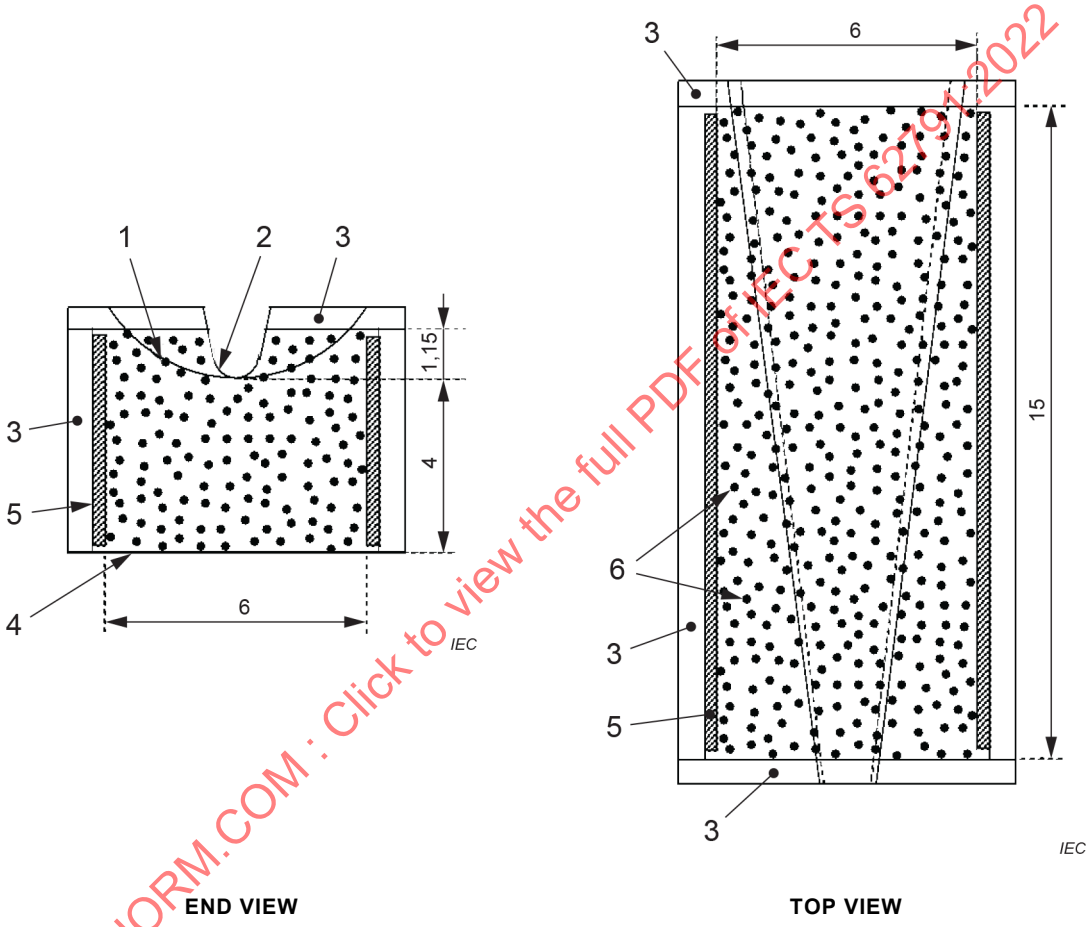

Key

1 3,5 cm radius of curvature
2 0,5 cm radius of curvature
3 6-mm-thick acrylic wall
4 flat screening window
5 3-mm-thick alumina reflector
6 2-mm-diameter −20 dB spheres (eight per millilitre)

Figure D.1 – End- and top-view diagrams of the phantom containing 2-mm-diameter, low-echo spheres with a backscatter level −20 dB relative to the background, for use in the 7 MHz to 23 MHz frequency range

This prototype phantom was produced with one plate-glass reflector and one parallel, alumina (Al_2O_3)-plate reflector. The alumina reflector has a very high density and acoustic propagation speed, providing total internal reflection for angles of incidence as small as 16°, as compared to about 30° for glass.

In Figure D.2, the C8-5 transducer designation implies that the pulse spectrum lies in the 5 MHz to 8 MHz range. The vertical set of echoes occur at the surface of the alumina reflector.

Figure D.2 – Image of the phantom containing 2-mm-diameter, −20 dB spheres [7], [8] obtained with a paediatric transducer with a radius of curvature of about 1,5 cm

Annex E
(informative)

Determination of low-echo sphere positions to within D/8 in x-, y- and z-Cartesian coordinates

E.1 Procedure

Preliminarily, the origin of the Cartesian coordinates will be addressed briefly. The origin should be placed at one of the points in the **cubic array**, where $(MPV)_{ijk}$-values are computed. k = 0 for the first image in the **image data set**; therefore, k = 0, 1, 2, …, $N_{\text{im}} - 1$, where N_{im} equals the number of images in the **image data set**. With reference to the definition of **depth interval** (3.9), Figure 1 and Figure B.2 d, the determination of **low-echo sphere** positions to within D/8 in x-, y- and z-Cartesian coordinates can be accomplished via the following steps [7].

NOTE 1 Since all Cartesian coordinates have a common factor of D/4, the convention is adopted that i, j and k without the D/4 factor are taken to mean the Cartesian coordinates iD/4, jD/4 and kD/4, respectively. Also, ijk means the **cubic array** site with coordinates iD/4, jD/4 and kD/4.

1) Using all digitized images and for each volume segment determined by the **depth interval label** d, compute the mean M_d and standard deviation σ_d of all MPVs with centres lying within the volume segment, using the entire image set. For images obtained with linear array transducers, d depends on the coordinate i, but for those obtained with sector probes, d is a function of both i and j (see Figure B.2 d).
2) For each $(MPV)_{ijk}$, identify the six nearest MPVs and determine whether all seven MPVs are at least 1,5 standard deviations below the mean established in step 1). Each such set of seven MPVs is taken to be associated with a **low-echo sphere**.
3) Typically, a set of seven MPVs determined in step 2) will overlap with other such sets of seven MPVs found in step 2). Associate each cluster of $(MPV)_{ijk}$'s – or, equivalently, each cluster of ijk's – and number the clusters n = 1, 2, 3, …, N_{o}. When a site is shared between two or more sets of seven MPVs or ijk's, that site counts as one site in the whole cluster of combined sets. When a set of seven MPVs or ijk's determined in step 2) does not overlap with another set of seven, then that set is the **cluster**.

   Consider, for example, the case in which two sets of seven MPVs or ijk's overlap regarding the j-coordinate as shown in the i,j plane in Figure E.1 (i, vertical; j, horizontal). Two positions designated with +'s are shared by the two sets.

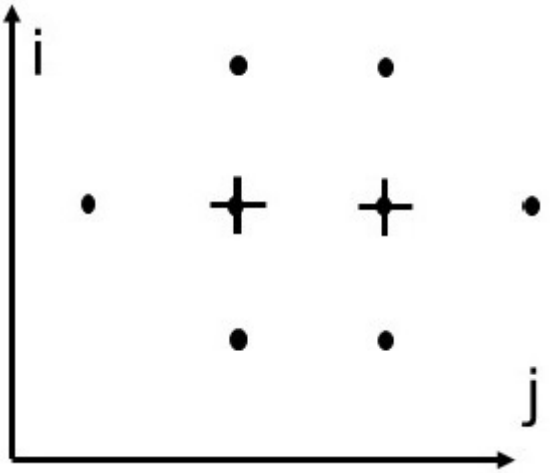

Figure E.1 – Diagram discussed in the second paragraph of 3)

The total number of positions for the computation in step 4) is then t_n (or t,n) = 8 + 4 = 12, the additional 4 being those positions in the adjacent elevational dimension.

4) For the nth cluster of MPVs or ijk's corresponding to step 3), compute the best estimate for the position of the nth **low-echo sphere** centre by computing the Cartesian coordinates of the "centre of mass" (x_{CMn}, y_{CMn} and z_{CMn}) as in Formulas (E.1), (E.2) and (E.3). Note that the summation is over all $(MPV)_{ijk}$ sites in the cluster, and each site is weighted by the factor $[M_{d(ij)n,s} - (MPV)_{(ijk)n,s}]$.

$M_{d(ij)n,s}$ is a very close approximation of the average over MPVs involving background alone. [See definition of $M_{d(ij)n,s}$ following Formulas (E.1), (E.2) and (E.3).]

$$x_{CMn} = \frac{\sum_{s=1}^{t,n} i(n,s)\frac{D}{4}\left[M_{d(ij)n,s} - (MPV)_{(ijk)n,s}\right]}{\sum_{s=1}^{t,n}\left[M_{d(ij)n,s} - (MPV)_{(ijk)n,s}\right]} \quad \text{(E.1)}$$

$$y_{CMn} = \frac{\sum_{s=1}^{t,n} j(n,s)\frac{D}{4}\left[M_{d(ij)n,s} - (MPV)_{(ijk)n,s}\right]}{\sum_{s=1}^{t,n}\left[M_{d(ij)n,s} - (MPV)_{(ijk)n,s}\right]} \quad \text{(E.2)}$$

$$z_{CMn} = \frac{\sum_{s=1}^{t,n} k(n,s)\frac{D}{4}\left[M_{d(ij)n,s} - (MPV)_{(ijk)n,s}\right]}{\sum_{s=1}^{t,n}\left[M_{d(ij)n,s} - (MPV)_{(ijk)n,s}\right]} \quad \text{(E.3)}$$

where

there are t_n (or t,n) sites in the nth cluster, the sites are numbered s = 1, 2, … t_n and (i,j,k) identifies the location of each of the t_n sites;

$(MPV)_{(ijk)n,s}$ is the MPV at the ijk-site in the cluster, as defined in 8.2;

$d(ij)n,s$ is a specific one of the **depth interval labels** (1, 2, 3 …, d_{max} – see 3.9.1); its value for each index in the summation depends on the cluster n and the coordinates (ij), the latter being determined by the integer s;

$M_{d(ij)n,s}$ is the mean of all MPVs with centres lying within a volume segment determined by the **depth interval label** d, using the entire image set, as defined above;

D is the diameter of the **low-echo spheres**, as defined in 3.4; D/4 is the distance between ijk points in the **cubic array**.

NOTE 1 d can take on different values, differing by ±1, in the summation when a cluster is shared between two adjacent **depth intervals**. For linear arrays, d has no j-dependence.

NOTE 2 Since 3,3 % or less of the tissue-mimicking material in the phantom consists of **low-echo spheres** (6.2.1.1 and 6.2.1.2), $M_{d(ij)n,s}$ is only slightly less than the mean value of pure background material.

Once the coordinates x_{CMn}, y_{CMn} and z_{CMn} of the centre of the nth **low-echo sphere** are found, this finding also determines the detected sphere's **depth interval label**, d. Spheres belonging to the same **depth interval** are included in computing "Mean LSNR"-values ($LSNR_{md}$) using Formula (3) in 8.4.2. The above process continues for all spheres detected, following steps 1) and 2) above.

E.2 Argument for the choice of seven *MPV* nearest-neighbour sites for determining the centres of low-echo spheres

Given that the sites involved should approximate a sphere with all sites lying inside a sphere of diameter D and all sites are at least 1,5 standard deviations (σ_d) below the mean (M_d) of all MPVs with centres lying within the volume segment determined by the **depth interval** d [see steps 1) and 2) in Clause E.1], the possibilities are as follows:

1) a single site;
2) eight sites at the corners of a cube with side D/4;
3) seven sites defining the centre and corners of a regular octahedron (as employed);
4) nine sites, one at the centre and eight on the corners of a cube with side D/2.

A single site (option 1) is unacceptable because random fluctuations in the background speckle would trigger an overwhelming number of false positives.

Option 2 is a possible choice with the greatest distance between two sites (at opposite corners of the cube) being $(3/16)^{1/2}\ D$ = 0,43 D.

For option 3 (the one used in the software), the maximum distance between sites is D/2, slightly greater than for option 2.

The maximum distance between sites for option 4 is $(3/4)^{1/2}\ D$ = 0,87 D. This distance is considered to be too large when considering finite beam widths in the lateral and elevational dimensions and finite pulse-length in the axial dimension – plus partial-volume effects due to the spherical geometry of the low-echo inclusions and the statistical nature of the speckle pattern; thus, it is unlikely that the MPVs at all eight corner sites would be less than $M_d - 1{,}5\ \sigma_d$ for less detectable **low-echo spheres**.

Using option 3, it was found that the number of **low-echo spheres** detected in any volume segment determined by the **depth interval** generally agrees with the mean number expected. Thus, almost all spheres detected by human observers in the image sets were detected by the software. Option 2 might be addressed in future research for comparison with option 3.

Annex F
(informative)

Tests of total internal reflection produced by alumina and plate-glass, plane reflectors

To test the effectiveness of the plate-glass and alumina reflectors at producing total internal reflection, such that for sufficiently small angles of incidence (90° being perpendicular incidence) mode conversion to shear waves or Rayleigh waves does not occur, a phantom was constructed with parallel alumina and plate-glass reflectors at opposite ends. The phantom was filled with tissue-mimicking background material (no **low-echo spheres**). The surfaces of the vertical plates were about 23 cm apart and two scanning windows existed on the top of the phantom. One scanning window had a 1 cm radius of curvature (ROC), half-cylindrical shape, centred 5 cm from the alumina reflector and the other was flat and had dimensions 5 cm × 10 cm with its centre line 5 cm from the plate-glass reflector. The curved window provided for coupling of a 1 cm-ROC curved array with a sector angle of about 153°, and the flat window allowed coupling of a phased array with a sector angle of about 90°. Thus, images could be created in which only one reflector was imaged and the other side of the image portrayed entirely tissue-mimicking material.

NOTE 1 The alumina reflector in the phantom described had a surface roughness of 6 µm, according to the manufacturer.

Regarding the tissue-mimicking material in the phantom, the component materials were the same as in the phantoms containing **low-echo spheres**, except that the volume percentage of 3:1 ultra-filtered milk was reduced by a factor of 4/5 to yield an (attenuation coefficient)/frequency value of $\alpha/f \approx 0{,}39$ dB cm^{-1} MHz^{-1} instead of 0,5 dB cm^{-1} MHz^{-1}, so that the penetration depth was greater, assuring availability of sufficient data for analyses. Measurements were carried out at 22 °C and 5 MHz using a previously described procedure [12]. The propagation speed was c = 1 539 m s^{-1}, and the attenuation factor was α/f = 0,39 dB cm^{-1} MHz^{-1} (see IEC 62391-1).

Figure F.1 shows an average over 10 images obtained by using the phased array. Two rectangular areas 10 mm wide represent areas where **mean pixel values** over 5 mm vertical-depth increments were computed. The plate-glass reflector is on the left (faint vertical line of diffuse reflections at the surface of the reflector). The reflector effectively extends the lateral region over which echoes will be detected. The rectangular ROI on the left is just beyond the plate-glass reflector, while the ROI on the right is inside the phantom.

NOTE 2 The **mean pixel value** in this Annex F does not refer to MPV over an area, A, as defined in 3.8. Here it is computed over 5 mm **depth intervals** within the rectangular regions on the images in Figure F.1.

The two rectangles have equal dimensions and are at the same positions vertically; however, one is just to the left of the vertical line of barely visible, diffuse reflections arising at the surface of the plate-glass reflector (left side in the image) and both rectangles are displaced by the same distance from the vertical axis of symmetry of the image. Thus, if total internal reflection were perfect and the imaging were perfect, then graphs of the **mean pixel values** over 5 mm vertical depth increments plotted against vertical depth would be identical for both rectangles. If there is asymmetry in the phased-array sensitivity, two such graphs would not be identical. Therefore, the transducer was rotated 180° about a vertical axis and another set of 10 images was obtained and averaged. With rotation of the transducer, the plate-glass reflector was located on the right side of the image.

Figure F.2 shows graphs of the **mean pixel values** plotted against depth for the left and right rectangles seen in Figure F.1. Note that the **mean pixel values** within the rectangles are zero for depths less than 5 cm and greater than 16 cm and are not shown. Figure F.3 shows the corresponding graphs after rotation of the transducer.

IEC

The scanning window is 5 cm from a plate-glass reflector, seen as a diffuse vertical line near the left side of the image.

Figure F.1 – Average of 10 images obtained by using a phased array transducer

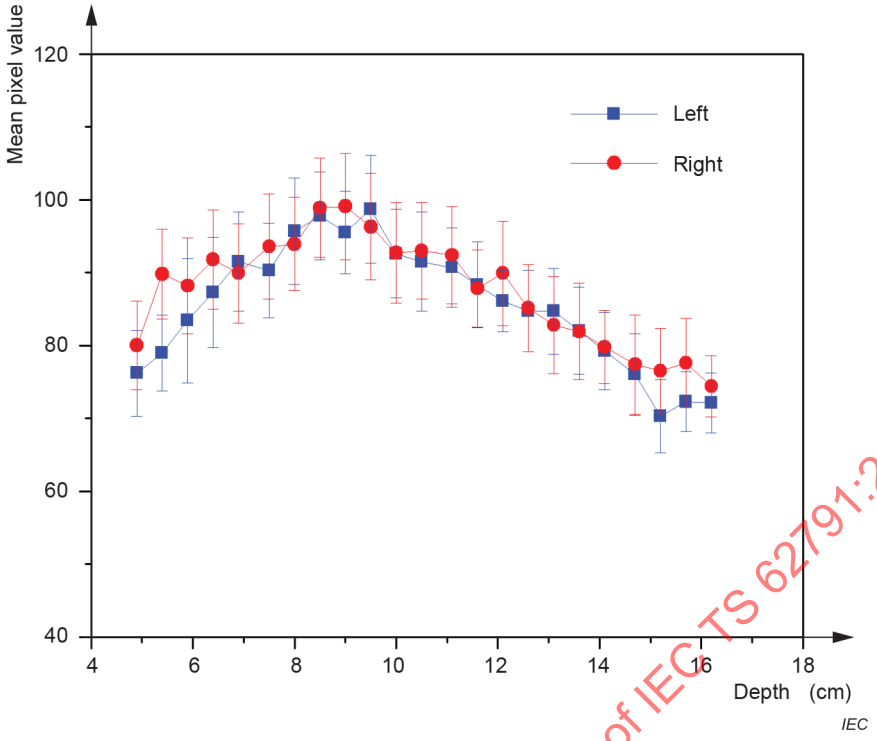

Blue data points (squares) were computed from pixel values in the left rectangle in Figure F.1 and red data points (circles) were computed from pixel values in the right rectangle.

Figure F.2 – Mean and standard deviation of pixel value plotted against depth from the two rectangular regions seen in Figure F.1

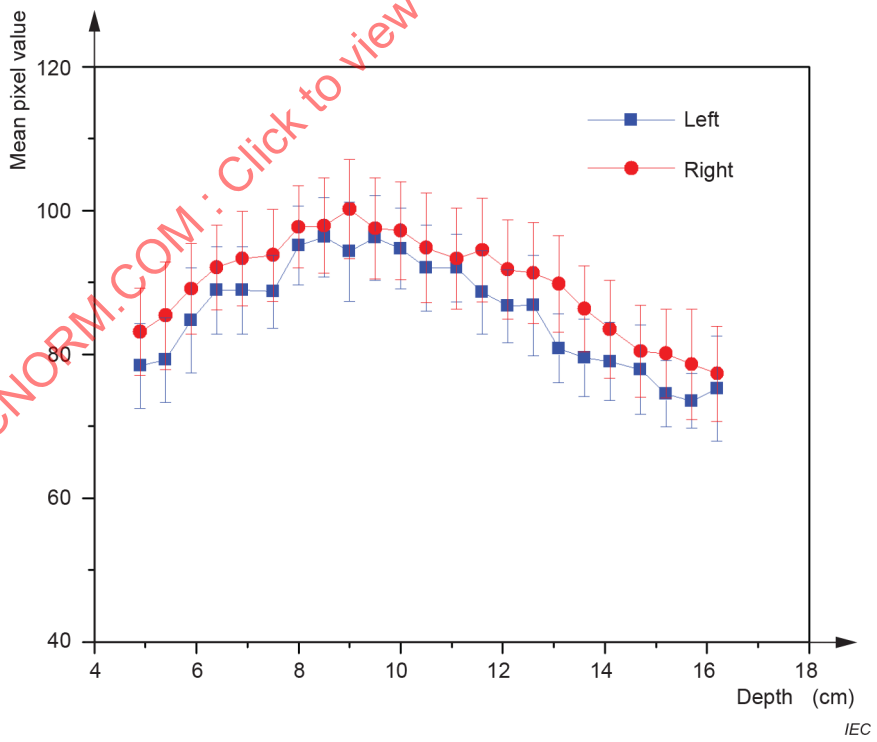

Blue points (squares) are mean pixel values for the left rectangle in Figure F.1 and red points (circles) are mean pixel values for the right rectangle, positioned just beyond the location of the alumina reflector.

Figure F.3 – Same as Figure F.2, but for data obtained after the transducer was rotated 180°, so the plate-glass reflector appeared on the right side of the image

The percentage by which the **mean pixel values** resulting from reflections differ from the **mean pixel values** not involving reflections, when asymmetry of transducer sensitivity is corrected, can be derived from the data in Figure F.2 and Figure F.3 using Formula (F.1).

$$\frac{1}{2}\sum_{i=1}^{2}\frac{R_i - N_i}{N_i}\times 100 \tag{F.1}$$

where

R_i and N_i are the **mean pixel values** on the reflector side and non-reflector side, respectively, and i = 1 corresponds to the reflector being on one side, and i = 2 corresponds to the reflector being on the other side.

The results appear in Figure F.4. In the data plotted here, asymmetry of transducer sensitivity has been corrected using the method just outlined.

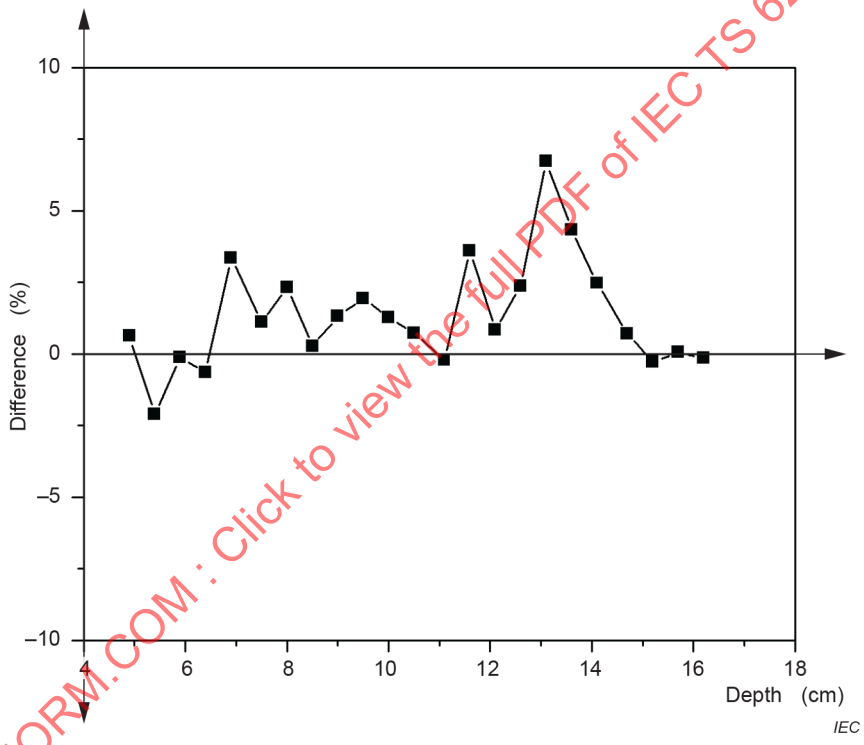

The reflector in this case is the plate-glass.

Figure F.4 – The percentage by which the mean pixel values resulting from reflections differ from the mean pixel values not involving reflections plotted against depth

Figure F.4 addresses the small contrast between the **mean pixel value** (corrected for transducer asymmetry) with both the alumina and plate-glass reflectors involved and the **mean pixel value** (corrected for transducer asymmetry) without involvement of the reflectors.

Figure F.5, Figure F.6 and Figure F.7 are analogous to Figure F.1, Figure F.2 and Figure F.3, except in this case the transducer is a curved array with a 1 cm radius of curvature, and the scanning window is closer to the alumina reflector. The sector angle is about 153°. Total internal reflection fails for sector angles greater than about 138°, corresponding to angles of incidence between 69° and 90°, as evidenced in the upper left side of the image in Figure F.5, distal to the reflector.